Full QCD hadron spectroscopy with two flavors of dynamical Kogut-Susskind quarks on the lattice

M. Fukugita
Yukawa Institute for Theoretical Physics, Kyoto University, Kyoto 606, Japan

N. Ishizuka
National Laboratory for High Energy Physics (KEK), Ibaraki 305, Japan

H. Mino
Faculty of Engineering, Yamanashi University, Kofu 400, Japan

M. Okawa
National Laboratory for High Energy Physics (KEK), Ibaraki 305, Japan

A. Ukawa
Institute of Physics, University of Tsukuba, Ibaraki 305, Japan
(Received 5 August 1992)

A full lattice QCD simulation is carried out with two flavors of Kogut-Susskind staggered dynamical quarks using lattices of a size ranging from 4^4 to 20^4 at the gauge coupling constant $\beta=6/g^2=5.7$ with the quark mass of $m_q=0.01$ and 0.02 in lattice units. Primary emphasis is given to the study of finite-lattice-size effects in the hadron mass spectrum. It is found that hadron masses suffer from substantial finite-size effects even for a lattice size of the order of 2 fm, showing the importance of a quantitative control of the effect for a comparison with the experimental spectrum at the accuracy of a few percent level. The finite-size correction is found to be well described by a power law in the lattice size, rather than an exponential form predicted by analytic formulas derived for point particles. It is suggested that the effect arises from the size of hadrons squeezed on a finite lattice. Finite-size effects on the realization of chiral symmetry are also studied. The behavior of the pion mass, the chiral condensate, and the mass splitting between parity partners all support a spontaneous breakdown of chiral symmetry for a large lattice size. Prediction from chiral Lagrangians on the size dependence of the chiral condensate does not describe the simulation results well, however, at least for the quark mass employed for the present study. Calculation of the pion decay constant with various relations derived from current algebra and partial conservation of axial-vector current gives $f_\pi=94(8)-105(9)$ MeV, with a method-dependent uncertainty contained within 10%. An examination is also made of the question of the dependence of hadron masses on hadron operators. Meson masses are basically operator independent, while baryon masses exhibit some operator dependence, necessitating further studies to resolve systematic uncertainties of this origin in the determination of the hadron mass spectrum.

PACS number(s): 12.38.Gc, 11.15.Ha

I. INTRODUCTION

The ultimate goal of numerical studies of QCD on a lattice is a quantitative understanding of the dynamics of strong interactions from first principles. Calculation of the hadron mass spectrum is a basic step toward this goal. Indeed, agreement of the calculated spectrum with experiment will provide an important verification of the correctness of QCD at low energies where nonperturbative dynamics dominate. At the same time, these calculations allow a determination of the physical scale which is needed to evaluate other physical quantities such as the transition temperature to the quark-gluon plasma phase and various weak matrix elements of phenomenological importance. For these reasons a large number of spectrum calculations have been attempted over the past decade, including full quark loop effects [1–7].

There are two sources of systematic errors inherent in lattice calculations of the hadron mass spectrum: the error arising from a finite lattice spacing and that due to a finite extent of the lattice. The importance has been widely realized for the first, and a lot of effort has been made toward a yet weaker coupling, examining the scaling behavior needed to take the continuum limit. The question of finite-size effect is also important since an examination of finite lattice spacing effect necessarily requires precise hadron mass data valid for infinite spatial volume. The recent quenched simulations [8–11] made some investigation of this problem. Typically employing two sets of lattice sizes, these simulations did not report a clear size-dependent shift in hadron masses for a physical lattice size of order 2 fm. For full QCD including dynamical quarks we started a systematic study of finite-size effects a few years ago. After the first report of the

work [12] the MILC Collaboration undertook a similar study at a larger lattice spacing [13]. Since finite-size effects should be more complex in the presence of dynamical sea quarks than in the quenched approximation, a detailed examination of the problem is an important step before a full QCD calculation of the hadron mass spectrum with a realistic predictive power can be realized.

Finite-lattice-size effects on hadron masses arise from various sources in QCD. The first source is whether the physical size of the lattice is large enough to contain hadrons, so that the hadron wave function is not artificially distorted. For a lattice size much larger than the hadron radius, we still expect finite-size effects arising from loops of virtual pions which wind around the lattice in the spatial direction [14,15]. An estimation using the general formula derived for point particles [14] or chiral perturbation theory [15] has been available, suggesting that this effect gives rise to a mass shift of the form $\exp(-cm_\pi L)$ with m_π the pion mass and L the spatial lattice size. The estimated magnitude of the shift is small for hadrons, and of the order of 1–2 % for a lattice size of $L \approx 2$ fm, rapidly diminishing for larger L.

There is yet another source of finite-size effects for small spatial sizes. It is well known that a spontaneous breakdown of symmetry does not occur at a finite volume. We expect that chiral symmetry, spontaneously broken for infinite volume, becomes restored as the lattice size diminishes [16,17]. This restoration is connected with a change of the nature of fluctuations of quark and gluon fields, which in turn affects hadron masses in a significant way. In particular one expects the pion to become heavier since its mass is no longer constrained by the Nambu-Goldstone theorem in the absence of spontaneous breakdown. Hadron masses other than that of the pion are also affected; the restoration of chiral symmetry causes a degeneracy of hadron masses of parity partners.

We have carried out a hadron mass spectrum calculation with two flavors of Kogut-Susskind (KS) staggered dynamical quarks with the primary purpose of studying finite-size effects. Our calculations have been made at the inverse coupling constant $\beta=6/g^2=5.7$ using two values of the quark mass $m_q=0.01$ and 0.02 in lattice units and employing lattices ranging from 4^4 to 20^4. Generation of gauge configurations was made by the hybrid R algorithm [18]. Hadron propagators were calculated using the hadron operators constructed in Refs. [19,20] using the technique of wall sources [21,10]. A brief description of our chief findings has already been published [12,22]. We have since augmented the statistics for a 20^4 lattice and we report in this article the full details of our simulations and results of analyses.

This paper is organized as follows. In Sec. II we describe the details of our simulation, including the choice of parameters for the hybrid R fermion algorithm, discussions of systematic errors of the algorithm and the question of autocorrelation among generated configurations. The list of runs we made and the average values of Wilson loops and the chiral order parameter are given. A brief description of the construction of hadron operators for Kogut-Susskind fermions and wall sources is also made. In Sec. III we present our data for hadron masses, following a description of the fitting procedure of hadron propagators and the method of error analyses. The dependence of masses on hadron operators is discussed, and the physical scale of the lattice spacing and the quark mass are examined. In Sec. IV we make a detailed study of finite-size effects for hadron masses and mass ratios. We present our results related to chiral symmetry in Sec. V. These include size effects in the chiral order parameter, the PCAC (partial conservation of axial-vector current) relation for the pion mass, and the pion decay constant. Our conclusions are summarized in Sec. VI.

II. FORMULATION AND METHOD OF MEASUREMENTS

A. Partition function

We study lattice QCD with two flavors of light dynamical quarks using the Kogut-Susskind fermion formalism. The Kogut-Susskind quark action is defined by

$$S_q=\sum_{n,n'}\bar{\chi}(n)D(U)_{n,n'}\chi(n') \tag{2.1}$$

with

$$D(U)_{n,n'}=m_q\delta_{n,n'}+\tfrac{1}{2}\sum_\mu \eta_\mu(n)[U_\mu(n)\delta_{n,n'-\mu} - U_\mu^\dagger(n-\mu)\delta_{n,n'+\mu}] , \tag{2.2}$$

where m_q is the quark mass in lattice units, $\eta_\mu(n)=(-1)^{n_1+n_2+\cdots+n_{\mu-1}}$ is the staggered sign factor, and $U_\mu(n)$ is the SU(3) link variable. Since this action is expected to describe four degenerate flavors of quarks in the continuum limit, we employ the conventional procedure of taking the square root of the quark determinant in the partition function to reduce the effective number of flavors to 2. We also use the well-known property of $D(U)$ that the product $D^\dagger(U)D(U)$ splits into two submatrices for even and odd sites. The system we study is thus defined by the partition function

$$Z=\int\prod_{n\mu}dU_\mu(n)e^{S_g(U)}\det[D^\dagger(U)D(U)]^{N_f/4} , \tag{2.3}$$

where the determinant is taken only over the subspace of even sites and the number of flavors N_f is set equal to 2. For the gauge action S_g we employ the single plaquette form given by

$$S_g=\beta\sum_{n,\mu,\nu}\mathrm{tr}[U_\mu(n)U_\nu(n+\mu)U_\mu^\dagger(n+\nu)U_\nu^\dagger(n)] , \tag{2.4}$$

where $\beta=6/g^2$ is the inverse gauge coupling constant squared.

B. Dynamical fermion algorithm and systematic errors

We employ the hybrid R algorithm [18] for generating an ensemble of gauge configurations including the effects of dynamical quarks. Our implementation of the algorithm follows that of Ref. [18]. The normalization of the

discretization time step $\delta\tau$ for molecular dynamics evolution is the same as in this reference, and integer and half-odd integer time steps are assigned to the link variables and the conjugate momenta, respectively, in the leapfrog integration of the molecular dynamics equations.

We use the conjugate gradient algorithm to invert the quark matrix needed in the molecular dynamics evolution. The equation to be solved is given by

$$D^\dagger(U)D(U)x = P_e D^\dagger(U')\xi \ , \tag{2.5}$$

where x is defined only on even sites, P_e is the projection onto even sites, ξ is a Gaussian random vector normalized as $\xi^a_n \xi^{b\dagger}_{n'} = \delta^{ab}\delta_{n,n'}$ with a and b the color indices, and U' is the link variable at the time $-N_f\delta\tau/8$ relative to that of U. To specify the stopping condition of the conjugate gradient iteration we define

$$r \equiv \left(\frac{\|D^\dagger(U)D(U)x - P_e D^\dagger(U')\xi\|^2}{3V} \right)^{1/2} , \tag{2.6}$$

with V the space-time lattice volume. The denominator equals the average of the norm squared of the source vector $\|P_e D^\dagger(U')\xi\|^2$ over the Gaussian random vector ξ for zero quark mass.

The hybrid R algorithm suffers from systematic errors of order $\delta\tau^2$ arising from a finite time-step size $\delta\tau$ as well as from the choice of the stopping condition of the conjugate gradient iteration. For all of our runs we use $\delta\tau=0.01$ for the quark mass $m_q=0.01$ and $\delta\tau=0.02$ for $m_q=0.02$ with the stopping condition $r<10^{-4}$ for both cases.

In order to examine whether our parameter choices are sufficient to avoid systematic errors several tests are carried on a 20^4 lattice at $m_q=0.01$ and $\beta=5.7$. We made a run of length $\tau=200$ with an increased step size $\delta\tau=1/70\sim 0.01\sqrt{2}$ starting from the configuration of the run with $\delta\tau=0.01$ at $\tau=500$. The time histories of the

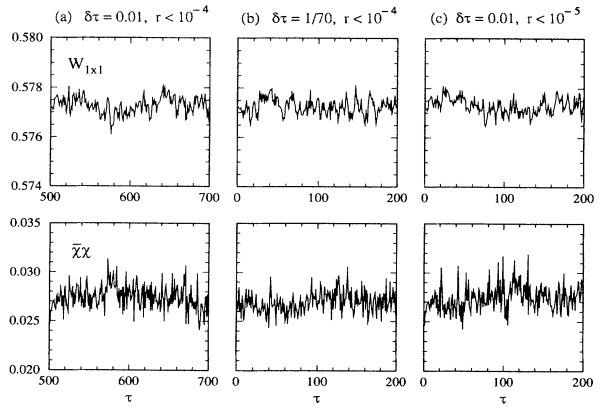

FIG. 1. Time histories of the 1×1 Wilson loop and chiral order parameter for several choices of the step size $\delta\tau$ and the stopping condition r for the conjugate gradient inversion of the quark operator on a 20^4 lattice at $\beta=5.7$ and $m_q=0.01$ with two dynamical flavors of KS fermions. (a) $\delta\tau=0.01$, $r<10^{-4}$, (b) $\delta\tau=1/70$, $r<10^{-4}$, (c) $\delta\tau=0.01$, $r<10^{-5}$. The runs in (b) and (c) are started from the configuration of (a) at $\tau=500$.

TABLE I. Comparison of Wilson loops and chiral order parameter for various choices of the step size $\delta\tau$ and the conjugate gradient stopping condition r in hybrid R runs on a 20^4 lattice at $\beta=5.7$ and $m_q=0.01$. All three runs start from the same configuration and averages are taken over the next 200 time units with errors estimated by the jack-knife method with a bin size of $\tau_{\rm bin}=50$.

$\delta\tau$	0.01	1/70	0.01
r	10^{-4}	10^{-4}	10^{-5}
$W_{1\times1}$	0.577 272(96)	0.577 247(35)	0.577 292(98)
$W_{2\times2}$	0.174 67(13)	0.174 624(72)	0.174 67(14)
$W_{3\times3}$	0.040 993(72)	0.040 994(42)	0.040 997(84)
$W_{4\times4}$	0.008 514(28)	0.008 529(30)	0.008 480(42)
$W_{5\times5}$	0.001 618(13)	0.001 627(14)	0.001 622(26)
$\langle\bar\chi\chi\rangle$	0.027 41(18)	0.026 94(20)	0.027 43(25)

1×1 Wilson loop and the chiral order parameter $\langle\bar\chi\chi\rangle$ (see Sec. II C below for our normalization and the method of computation) for the two runs are compared in Figs. 1(a) and 1(b), and their average values are given in Table I. Analytical results predicting the sign and magnitude of finite step size errors are not available. An

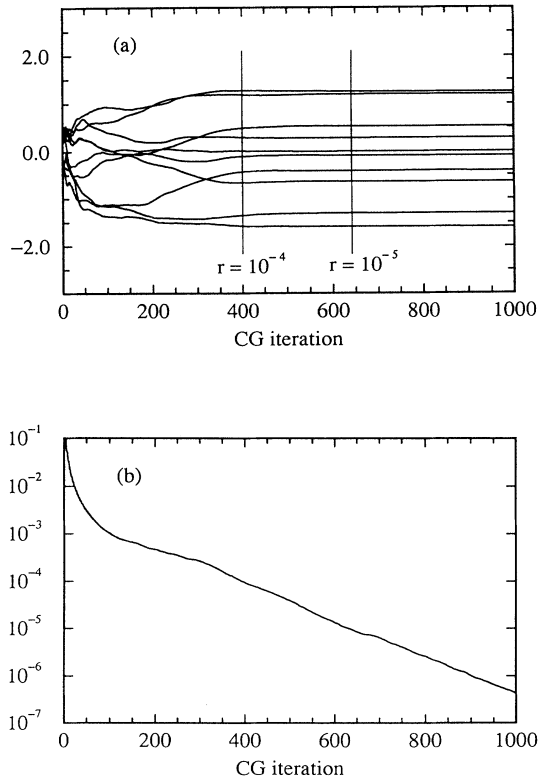

FIG. 2. (a) Convergence of the solution vector x for $D^\dagger D(U)x = P_e D^\dagger(U')\xi$ as a function of the number of conjugate gradient iterations on a 20^4 lattice at $\beta=5.7$ and $m_q=0.01$. Ten elements randomly chosen are shown. (b) Norm $r=\|D^\dagger Dx - P_e D^\dagger\xi\|/\sqrt{3V}$ as a function of the number of conjugate gradient iterations.

empirical study [23] shows, however, that the Wilson loops decrease and the chiral order parameter increases for a larger step size. Such deviations are not apparent in the time histories in Fig. 1 and average values in Table I. Indeed the average values of the two runs are consistent [24].

In Fig. 2 we show several elements of the solution vector x of (2.5) and the normalized residual r defined by (2.6) as a function of the number of conjugate gradient iterations from a configuration of the run with $\delta\tau=0.01$. We observe a slight change for some elements beyond $r=10^{-4}$ used for our runs. The possible significance of these changes is tested by a run of length $\tau=200$ with $\delta\tau=0.01$ using a more strict stopping condition $r<10^{-5}$, which is started from the configuration of the run with $\delta\tau=0.01$ at $\tau=500$. As is seen in Figs. 1(a) and 1(c) and Table I we do not observe a clear deviation of average values from the case of the stopping condition $r<10^{-4}$.

We conclude that our choice of the step size and the stopping condition are probably sufficient, at least at the level of statistics we could generate with our present computer resources.

C. Runs

We have generated ensembles of gauge configurations at $\beta=5.7$ with the quark mass of $m_q=0.01$ and 0.02 for various lattice sizes ranging from 4^4 to 20^4. The periodic boundary condition is taken in all directions for both gauge and quark fields. For all of our runs we used the step size of $\delta\tau=0.01$ for $m_q=0.01$ and $\delta\tau=0.02$ for $m_q=0.02$ with one trajectory corresponding to $\tau=1$, and the stopping condition for inverting the fermion matrix is taken to be $r<10^{-4}$. Most of our computing time was devoted to the runs on a 20^4 lattice. Simulations for smaller lattice sizes 4^4, 6^4, $8^3\times16$, 12^4, and 16^4 were made for a finite-size study of hadron masses and chiral symmetry. We did not pursue a long run on a 16^4 lattice because high statistics data on a $16^3\times32$ lattice became available from the Columbia group [4] in the course of our studies. We also made simulations of limited statistics at $\beta=5.4$, 5.5, and 5.6 for a preliminary study of lattice spacing dependence of local observables.

In the course of runs we measured Wilson loops and the chiral order parameter $\langle\bar{\chi}\chi\rangle$ at every $\tau=1$. Our normalization of $\langle\bar{\chi}\chi\rangle$ is given by

$$\langle\bar{\chi}\chi\rangle=\frac{1}{3}\mathrm{tr}\left[\frac{1}{D}\right]=\frac{m_q}{3}\mathrm{tr}\left[\frac{1}{D^\dagger D}\right]. \tag{2.7}$$

We used the noisy estimator $\mathrm{tr}(1/D^\dagger D)=\eta^\dagger(D^\dagger D)^{-1}\eta/(3V/2)$ with η a Gaussian noise vector $(\eta^a_n\eta^{b\dagger}_{n'}=\delta^{ab}\delta_{n,n'})$ for even sites, evaluating $(D^\dagger D)^{-1}\eta$ with the conjugate gradient method with the stopping condition $\|D^\dagger Dx-\eta\|/\sqrt{3V}<10^{-3}$.

In Table II we summarize the length of runs and the interval used for calculating averages in time units. Since the publication of our brief report [22] we have added 300 time units for a 20^4 lattice at $m_q=0.02$ and 50 time units at $m_q=0.01$. The choice of the averaging interval in Table II will be discussed in Sec. II E. Hadron propagators are evaluated at every 5 time units except for the runs on a 16^4 lattice at $\beta=5.7$ and those for $\beta<5.7$. The number of gauge configurations used for hadron propagator calculations are also listed in Table II.

D. Hadron propagators

1. *Hadron operators*

For Kogut-Susskind fermions the construction of hadron operators with definite spin-flavor quantum numbers is complicated due to the embedding of flavor and spin degrees of freedom onto lattice sites. This problem was studied in detail by Golterman and Smit some time ago [19,20] (see also Ref. [25]), and we follow their method and notations in this work.

Hadronic states at zero spatial momentum made out of Kogut-Susskind quarks can be classified by the irreducible representations of the group of transformations that commute with the transfer matrix T for Kogut-Susskind fermions, the rest-frame group [19,20]. The irreducible representations are labeled by their dimension **r**, parity

TABLE II. Length of runs in time units carried out for the present work. The first number denotes the number of time units discarded for thermalization, and the second number represent time unit intervals used for taking averages. Number of configurations used for hadron propagator calculations are given in parentheses.

β	5.7		5.6		5.5		5.4
m_q	0.01	0.02	0.01	0.02	0.01	0.02	0.01
4^4	100+900						100+900
6^4	100+900						100+900
8^4			100+900		100+900		100+1000
$8^3\times16$	200+800 (160)	200+800 (160)					
10^4					100+200 (20)		
12^4	300+700 (140)	300+700 (140)	100+200 (20)				100+200
16^4	250+250 (25)	200+300 (30)	100+200 (20)	100+100 (10)	100+100 (10)	100+100 (10)	
20^4	250+750 (150)	200+800 (160)					

σ_s under the space inversion and another parity σ_t for the transformation $\Xi_4=S_4T^{-1/2}$ with S_4 the unit shift in the time direction and $T=S_4^2$ the transfer matrix. The parity P in the continuum is identified with the product $P=\sigma_s\sigma_t$. Mesonic states fall into **1**, **2**, **3**, and **6** representations (there are two inequivalent **1**'s and six **3**'s), while baryonic states form **8**, **8'**, and **16**. The assignment of spin-flavor quantum number to these irreducible representations is made through their decomposition in terms of those of the $SU(4)_{\text{flavor}}\times SU(2)_{\text{spin}}$ group in the continuum, of which the rest-frame group is a subgroup. Based on this analysis the lowest state that couples to the baryonic **8** and **16** is considered to be the nucleon and that for **8'** the Δ baryon.

Hadron operators for Kogut-Susskind quarks constructed in Refs. [19,20] are generally extended over a four-dimensional hypercube. In our work we use only those operators which are local in time. In this case it is not possible to construct operators that carry a definite σ_t parity because of the nonlocal factor $T^{-1/2}$ in the Ξ_4 transformation. These operators therefore create both positive and negative continuum parity states in general. There are $8\times 8=64$ meson operators and ${}_8H_3=120$ baryon operators belonging to this class. The meson operators, consisting of 20 irreducible representations, take the form

$$\sum_{\mathbf{n}} s(n,\delta)\bar{\chi}(n)\chi(n+\delta)\ , \tag{2.8}$$

where $s(n,\delta)$ is a sign factor which is tabulated in Table 2a of Ref. [19]. The spin-flavor content of (2.8) is most easily found by transforming the KS fermion bilinear in (2.8) into Dirac bilinears of the form $\bar{q}\gamma_s\otimes\xi_f q$ where γ_s and ξ_f represent spinor and flavor γ matrices. The result is given in Table 5 of Ref. [19].

The 120 baryon operators fall into five **8**'s, four **16**'s, and two **8**''s. A representative of each of these eleven representations (two for each **16**'s) is explicitly given in Table 3 of Ref. [20], while the rest of the operators can be generated from these 15 operators by application of spatial rotations and translations. The 15 operators are given by linear combinations of the operators $O^{(i)}$,

$$\begin{aligned}
O^{(1)}&=\sum_{\mathbf{n}\in(2\mathbb{Z})^3}\chi(n)\chi(n)\chi(n)\ ,\\
O_k^{(2)}&=\frac{1}{2}\sum_{\mathbf{n}\in(2\mathbb{Z})^3}\sum_{\delta=\pm\hat{\mathbf{k}}}\chi(n)\chi(n+\delta)\chi(n+\delta)\ ,\\
O_k^{(3)}&=\frac{1}{4}\sum_{\mathbf{n}\in(2\mathbb{Z})^3}\sum_{\delta=\pm\hat{l}\pm\hat{\mathbf{m}}}\chi(n)\chi(n+\delta)\chi(n+\delta)\ ,\\
O_k^{(4)}&=\frac{1}{8}\sum_{\mathbf{n}\in(2\mathbb{Z})^3}\sum_{\delta_1=\pm\hat{\mathbf{k}},\delta_2=\pm\hat{l},\delta_3=\pm\hat{\mathbf{m}}}\\
&\quad\pm\chi(n+\delta_1)\chi(n+\delta_1+\delta_2)\chi(n+\delta_1+\delta_3)\ ,\\
O^{(5)}&=\sum_{\mathbf{n}\in(2\mathbb{Z})^3}\chi(n)\chi(n)\chi(n+\hat{1}+\hat{2}+\hat{3})\ ,\\
O_k^{(6)}&=\frac{1}{8}\sum_{\mathbf{n}\in(2\mathbb{Z})^3}\sum_{\delta_1=\pm\hat{\mathbf{k}},\delta_2=\pm\hat{l}\pm\hat{\mathbf{m}}}\pm\chi(n)\chi(n+\delta_1)\chi(n+\delta_2)\ ,\\
O^{(7)}&=\chi(n+\hat{1})\chi(n+\hat{2})\chi(n+\hat{3})\ ,
\end{aligned}\tag{2.9}$$

where (k,l,m) is a cyclic permutation of (1,2,3) with $\hat{\mathbf{k}}$ the unit vector in the spatial direction k, and $\pm$ in the operators $O^{(4)}$ and $O^{(6)}$ means that $\chi(n\pm\hat{1}\pm\hat{3})$ should be multiplied by -1 [20].

We calculate hadron propagators using the 64 meson operators and the 15 baryon operators as sink. A technical complication here is that clear signals can be seen only when a source suitable for individual operators is selected. With our choice of source, to be described below, we expect a good signal-to-noise ratio for the propagators of 11 meson operators and 11 baryon ones. The explicit form of these operators and the representation labels of hadronic states $(\mathbf{r},\sigma_s,\sigma_t)$ that couple to them are listed in Table III using the notation of (2.8) and (2.9) (for mesons the parity σ_{123} under $\Xi_1\Xi_2\Xi_3$ is also attached where $\Xi_\mu=S_\mu T^{-1/2}$ with S_μ the unit translation in the direction μ). In this table our convention for the naming of operators is as follows: we use roman numerals to number the 20 meson irreducible representations according to the order with which they are listed in Table 5 of Ref. [19] and similarly for the 11 baryon irreducible representations in Table 3 of Ref. [20]. Subscripts of roman numerals in Table III distinguish members within an irreducible representation. Each operator couples to two states having an opposite continuum parity $P=\sigma_s\sigma_t$. For mesonic states the spin-flavor content in terms of the spin-flavor Dirac matrices $\gamma_s\otimes\xi_f$ and the name of particles are given. The conventional notation of Ref. [26] for local meson operators $M(I)-M(IV)$ is also attached.

The particle states in Table III include the Nambu-Goldstone pion $\pi(\gamma_5\xi_5)$ associated with the U(1) chiral symmetry of the Kogut-Susskind fermion action and two other members of the pion multiplet $\pi(\gamma_4\gamma_5\xi_4\xi_5)$ and $\pi(\gamma_5\xi_3\xi_5)$. The parity partners of $\pi(\gamma_5\xi_5)$ and $\pi(\gamma_5\xi_3\xi_5)$ have the quantum number $J^{PC}=0^{+-}$ which is not allowed in quark models. There are eight ρ mesons with various flavor quantum numbers. The nucleon appears in a number of channels $B(\text{I})-B(\text{IV})$ and $B(\text{VII})-B(\text{X})$. Among them the operator $B(\text{I})$ is the conventional local nucleon operator. The Δ baryon is expected to be the lowest state that couples to the operators $B(\text{VI})$ and $B(\text{XI})$ [20]. The states $\pi(\gamma_5\xi_5)$, $\rho(\gamma_k\xi_k)$, and the nucleon created by the conventional local nucleon operator $B(\text{I})$ will be denoted as π, ρ, and N.

2. *Wall sources*

Hadron masses are extracted from the exponential decay of the two-point function of a hadronic source and a sink at a large time separation. In order to enhance signals of the lightest states that contribute to the hadron propagators we employ the technique of wall sources [21,10]. In this method one uses a quark source of the form $\sum_{\mathbf{n}}\bar{\chi}(\mathbf{n};t=0)W(\mathbf{n})$ with $W(\mathbf{n})$ the amplitude of the source, which is extended over the $t=0$ time slice. Hadron propagators are constructed by substituting the quark propagator $G^W(n)=D^{-1}_{n,n'}W_{n'}$ for the source W into $\chi(n)$ and $\epsilon(n)G^{W*}(n)$ with $\epsilon(n)=(-1)^{n_1+n_2+n_3+n_4}$ for $\bar{\chi}(n)$ in the hadron operators of Table III.

Improvement of signals with wall sources arises from

the fact that hadrons are emitted from each site on the $t=0$ time slice, and therefore the weight of the zero-momentum component is enhanced. In principle one can further improve the signal by an appropriate choice of the wall source so that only states carrying the same quantum numbers as that of the operator at the sink are created [27]. To see this let α^i $(i=1,\ldots,8)$ be the vector corresponding to the 8 vertices of a unit spatial cube and define 8 types of wall sources by

$$W_i(\mathbf{n})=\sum_{\mathbf{m}\in(2\mathbb{Z})^3}\delta_{\mathbf{n},\mathbf{m}+\alpha^i}\ . \tag{2.10}$$

Clearly any basis of the irreducible representations of operators local in time can be constructed by an appropriate linear combination of hadronic source operators given by

$$\begin{aligned}\mathcal{O}^{ij}_{\text{meson}}&=\sum_{\mathbf{n},l}\bar{\chi}(\mathbf{n};t=0)\chi(l;t=0)W_i(\mathbf{n})W_j^{\dagger}(l)\epsilon(l)\ ,\\ \mathcal{O}^{ijk}_{\text{baryon}}&=\sum_{\mathbf{n},l,\mathbf{m}}\bar{\chi}(\mathbf{n};t=0)\bar{\chi}(l;t=0)\bar{\chi}(\mathbf{m};t=0)\\ &\quad\times W_i(\mathbf{n})W_j(l)W_k(\mathbf{m})\ .\end{aligned} \tag{2.11}$$

In practice, however, this procedure requires much computer time since 8 quark propagators have to be computed for each gauge configuration. In this work we therefore use only two types of wall source.

The wall sources we use are defined by

$$\begin{aligned}W^a(\mathbf{n})&=1\ ,\\ W^e(\mathbf{n})&=\begin{cases}1 & \text{for } n_i=0 \bmod 2,\\ 0 & \text{otherwise}\ .\end{cases}\end{aligned} \tag{2.12}$$

It is straightforward to find the hadronic states created by these wall sources by inspecting the overlap of the source operator (2.11) with $W=W^a$ or W^e with the hadron operators discussed in Sec. II D 1. The result is shown in the last column of Table III. The a source emits mesons corresponding to the operators with the sign factor $\epsilon(\mathbf{n})$. All local mesons are emitted by the e source. The Nambu-Goldstone pion $\pi(\gamma_5\xi_5)$ is observed for both sources. We adopted the a source for this channel because we obtained better signals than for the e source. For baryons 4 operators out of the 15 we study have no overlap with neither of our source, and we observed signals for the remaining 11 operators listed in Table III. The e source has an overlap only with the local nucleon operator $B(I)$, while the a source create signals for all the operators in Table III. The local nucleon can be observed for both sources, and we adopted the e source for the better quality of signals.

TABLE III. Kogut-Susskind hadron operators used for the present work. Representation labels [19,20] and particles that couple to the operators are listed. See the text for the convention for names of operators and the meaning of symbols. For local meson operators M(I)–M(IV) the conventional notation of Ref. [26] is also given. The last column gives the type of wall source used for calculating the corresponding hadron propagator.

(a) Mesons

	δ	$s(n,\delta)$	$\mathbf{r}^{\sigma_{123}}$	σ_s	$\sigma_t=+1$	$\sigma_t=-1$	Source
M(I) (SC)	0	1	$\mathbf{1}^+$	+1	$\sigma^{++}(1)$	$\pi(\gamma_4\gamma_5\xi_4\xi_5)$	e
M(II) (PS)	0	$\epsilon(\mathbf{n})$	$\mathbf{1}^-$	+1	$0^{+-}(\gamma_4\xi_4)$	$\pi(\gamma_5\xi_5)$	a
M(III) (PV)	0	$(-1)^{n_k}$	$\mathbf{3}''''^-$	+1	$a_1(\gamma_k\gamma_5\xi_k\xi_5)$	$\rho(\gamma_k\gamma_4\xi_k\xi_4)$	e
M(IV) (VT)	0	$(-1)^{n_k}\epsilon(\mathbf{n})$	$\mathbf{3}''''^+$	+1	$b_1(\gamma_l\gamma_m\xi_l\xi_m)$	$\rho(\gamma_k\xi_k)$	e
M(VI)	$\hat{1}$	$\epsilon(\mathbf{n})$	$\mathbf{3}^-$	−1	$\rho(\gamma_1\gamma_4\xi_4)$	$a_1(\gamma_1\gamma_5\xi_5)$	a
M(VII)	$\hat{3}$	$\epsilon(\mathbf{n})$	$\mathbf{3}^+$	−1	$\pi(\gamma_5\xi_3\xi_5)$	$0^{+-}(\gamma_4\xi_3\xi_4)$	a
M(X)	$\hat{2}$	$\epsilon(\mathbf{n})$	$\mathbf{6}^+$	−1	$\rho(\gamma_3\xi_2\xi_3)$	$b_1(\gamma_1\gamma_2\xi_1)$	a
M(XV$_1$)	$\hat{2}+\hat{3}$	$\epsilon(\mathbf{n})$	$\mathbf{6}^+$	+1	$b_1(\gamma_1\gamma_2\xi_1\xi_3)$	$\rho(\gamma_3\xi_2)$	a
M(XV$_2$)	$\hat{1}+\hat{2}$	$\epsilon(\mathbf{n})$	$\mathbf{6}^+$	+1	$b_1(\gamma_1\gamma_3\xi_2\xi_3)$	$\rho(\gamma_2\xi_1)$	a
M(XVI)	$\hat{3}+\hat{1}$	$\epsilon(\mathbf{n})$	$\mathbf{6}^-$	+1	$a_1(\gamma_1\gamma_5\xi_3\xi_5)$	$\rho(\gamma_1\gamma_4\xi_3\xi_4)$	a
M(XX)	$\hat{1}+\hat{2}+\hat{3}$	$\epsilon(\mathbf{n})$	$\mathbf{3}''''^+$	−1	$\rho(\gamma_2\xi_3\xi_1)$	$b_1(\gamma_1\gamma_3\xi_2)$	a

(b) Baryons

	Weight	$\mathbf{r}$	σ_s	$\sigma_t=+1$	$\sigma_t=-1$	Source
B(I)	$O^{(1)}$	**8**	+1	N	N^-	e
B(II)	$O_1^{(2)}+O_2^{(2)}+O_3^{(2)}$	**8**	+1	N	N^-	a
B(IV)	$O_1^{(3)}+O_2^{(3)}+O_3^{(3)}$	**8**	+1	N	N^-	a
B(VI)	$O_1^{(4)}+O_2^{(4)}+O_3^{(4)}$	**8′**	−1	Δ^-	Δ	a
B(VII$_1$)	$O_1^{(4)}-O_2^{(4)}$	**16**	−1	N^-	N	a
B(VII$_2$)	$O_1^{(4)}+O_2^{(4)}-2O_3^{(4)}$	**16**	−1	N^-	N	a
B(VIII)	$O^{(5)}$	**8**	−1	N^-	N	a
B(IX)	$O_1^{(6)}+O_2^{(6)}+O_3^{(6)}$	**8**	−1	N^-	N	a
B(X$_1$)	$O_1^{(6)}-O_2^{(6)}$	**16**	−1	N^-	N	a
B(X$_2$)	$O_1^{(6)}+O_2^{(6)}-2O_3^{(6)}$	**16**	−1	N^-	N	a
B(XI)	$O^{(7)}$	**8′**	−1	Δ^-	Δ	a

3. *Hadron propagator calculations*

A reliable extraction of masses of lowest hadronic states requires a large temporal separation between a source and a sink. Since most of our gauge configurations are generated on space-time symmetric lattices, we periodically duplicate or triplicate gauge configurations in the time direction so that the temporal lattice size is 32 or larger.

Hadron operators and wall sources described above are generally not gauge invariant. We therefore fix link variables to a gauge. We choose a hybrid gauge in which all the links on the original lattice is fixed to the Landau gauge through a maximization of

$$F_L = \sum_{n,\mu} \mathrm{tr}[U_\mu(n) + U_\mu^\dagger(n)] \tag{2.13}$$

and, after multiplication of the lattice in the temporal direction, the spatial links on the $t=0$ time slice at the wall is further fixed to the Coulomb gauge by maximizing

$$F_C = \sum_{n,i} \mathrm{tr}[U_i(n) + U_i^\dagger(n)] \ . \tag{2.14}$$

The maximization of F_L and F_C is carried out by the naive steepest-descent method. For the Landau-gauge fixing 5000 iterations are made, which roughly correspond to the condition

$$\theta \equiv \frac{1}{V} \sum_n \mathrm{tr}[\Delta(n)\Delta^\dagger(n)] < 10^{-8} \ , \tag{2.15}$$

where V is the space-time lattice volume and

$$\Delta(n) = \sum_\mu [U_\mu(n-\hat{\mu}) - U_\mu(n) - \mathrm{H.c.} - \mathrm{trace}] \ . \tag{2.16}$$

We also made 5000 iterations for the Coulomb-gauge fixing of the $t=0$ time slice.

A potential difficulty with calculations of gauge noninvariant operators on gauge fixed configurations is the problem of Gribov copies [28]. To examine this problem we repeated maximization of F_L and F_C after random gauge transformations of link variables. We found that the presence of more than one local maximum is not a rare occurrence for many of the gauge configurations in our ensemble (see Ref. [29] for reports of a similar finding). In our preliminary investigation we found that the variation of hadron propagators for different maxima is within statistical fluctuations and that a systematic shift of hadron masses is not apparent. We therefore do not pursue this problem in the present work.

Quark propagator G^W for a wall source W is evaluated by writing $G^W = D^\dagger x$ and solving

$$DD^\dagger x = W \tag{2.17}$$

by the conjugate gradient algorithm for the subspaces of even and odd sites separately. We used the stopping condition

$$r_W \equiv \frac{\|W - DD^\dagger x\|}{3V_W} < 10^{-7} \tag{2.18}$$

with V_W the number of source points, i.e., $V_W = L^3/2$ for the a source and $L^3/8$ for the e source. With this condition hadron propagators are calculated at the accuracy of 0.001% for all the elements. As an illustration we show in Fig. 3 the propagator of the Nambu-Goldstone pion at several time separations and the norm of the residual vector r_W as a function of the number of conjugate-gradient iterations on a $20^3 \times (20 \times 2)$ configuration at $\beta = 5.7$ and $m_q = 0.01$.

E. Thermalization and autocorrelation

Error estimation requires a study of initial thermalization and autocorrelation in the set of generated gauge configurations. For our runs on a 20^4 lattice at $\beta = 5.7$ with $m_q = 0.01$ and 0.02 we show the time histories of $l \times l$ Wilson loops for $l = 1-5$, chiral order parameter $\langle \bar{\chi}\chi \rangle$, and π, ρ, and nucleon propagators at $t = 10$ in Fig. 4. These runs are started from a completely ordered configuration. The Wilson loops and the chiral order parameter approach thermalized values quickly after about 100 to 150 time units for both $m_q = 0.01$ and 0.02. Thermalization is about a factor of 2 slower for hadron propagators, taking about 250 to 300 time units for $m_q = 0.01$ and 150 to 200 units for $m_q = 0.02$. From these observations we choose to discard the initial 250 time units for $m_q = 0.01$ and 200 units for $m_q = 0.02$. The number of discarded initial time intervals for other

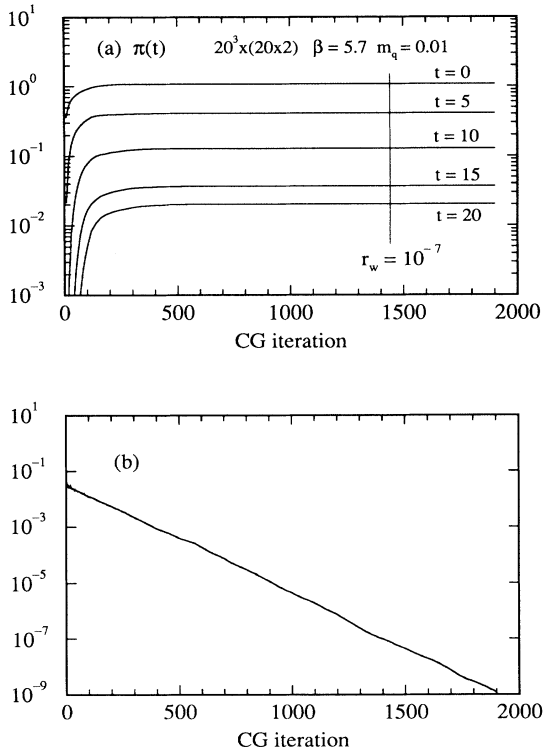

FIG. 3. (a) Convergence of the propagator $\pi(t)$ for local pion $\pi(\gamma_5\xi_5)$ with the a wall source on a $20^3 \times (20 \times 2)$ lattice at $\beta = 5.7$ and $m_q = 0.01$ as a function of the number of conjugate gradient iterations. Curves for several values of t are shown. (b) Norm $r_W = \|DD^\dagger x - W\|/3V_W$ as a function of the number of conjugate gradient iterations.

lattice sizes and parameters are chosen by similar analyses (see Table II).

One can study the magnitude of correlation between successive configurations through the autocorrelation function defined by

$$A_O(\tau_s)=\frac{\overline{O(\tau)O(\tau+\tau_s)}-\overline{O(\tau)}\,\overline{O(\tau+\tau_s)}}{\overline{O(\tau)^2}-\overline{O(\tau)}^2} \tag{2.19}$$

for an observable O where the bars denote average over τ from $\tau_{\min}$ to $\tau_{\max}-\tau_s$ with $\tau_{\min}$ the discarded time interval and $\tau_{\max}$ the total simulation time. In Fig. 5 we plot the autocorrelation functions at $m_q=0.01$ for various quantities whose time histories are shown in Fig. 4. We observe that the autocorrelation for the 1×1 Wilson loop decays quickly, becoming consistent with zero around $\tau_s\approx20$. For the chiral order parameter the correlation persists longer till $\tau_s\approx50-100$. A similar range of correlation is seen for the pion propagator. The autocorrelation functions for other hadron correlators decay more quickly, reflecting their noisier time histories.

The range of autocorrelation can also be analyzed by the jack-knife error analysis [30]. We divide the ensemble of configurations into $N_{\rm bin}$ bins with each bin extended over a time interval $\tau_{\rm bin}$ and define the error as a function of $\tau_{\rm bin}$ through

$$E_O(\tau_{\rm bin})=\left\{(N_{\rm bin}-1)\left[\left[\frac{1}{N_{\rm bin}}\sum_i O_i^2\right]-\left[\frac{1}{N_{\rm bin}}\sum_i O_i\right]^2\right]\right\}^{1/2}, \tag{2.20}$$

where O_i denotes the average obtained without the ith bin. One expects $E_O(\tau_{\rm bin})$ to reach a plateau when the bin size $\tau_{\rm bin}$ becomes comparable to or larger than the autocorrelation time. The height of the plateau provides an estimate of the error for the given ensemble taking into account autocorrelation. The bin size dependence of $E_O(\tau_{\rm bin})$ for various quantities for the run on a 20^4 lattice at $\beta=5.7$ and $m_q=0.01$ is plotted in Fig. 6. The results are in accord with those of the autocorrelation function analysis in that the errors are almost saturated for the bin size $\tau_{\rm bin}\approx50$. Based on these analyses we employed the jack-knife formula (2.20) with the bin size of $\tau_{\rm bin}=50$ for estimating errors of our data including those of hadron propagators. For short runs at $\beta<5.7$ with the simulation length $\tau<500$ we took the bin size $\tau_{\rm bin}=20$, however.

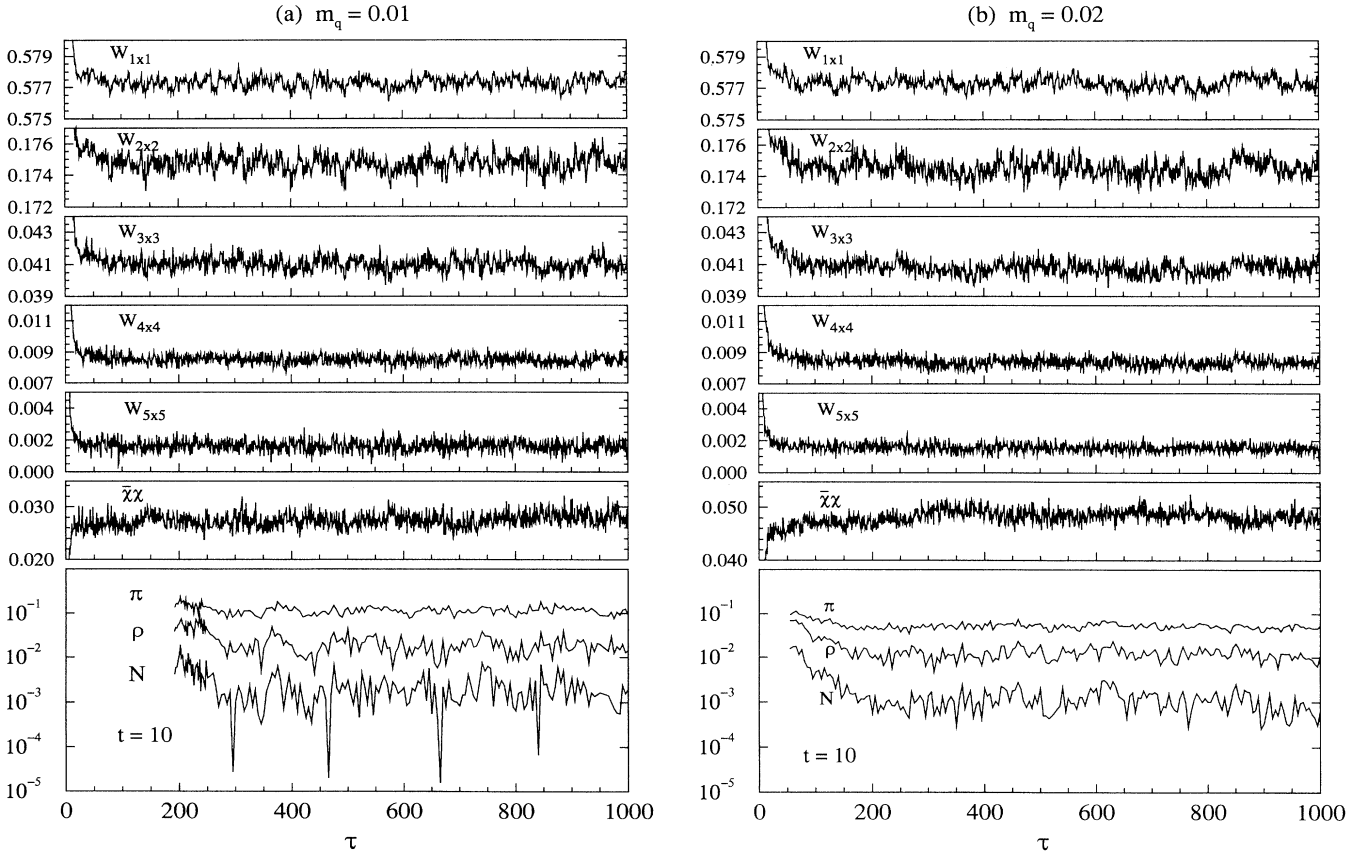

FIG. 4. Time histories of Wilson loops, chiral order parameter $\bar\chi\chi$, and $\pi(\gamma_5\xi_5)$, $\rho(\gamma_k\xi_k)$, and local nucleon (N) propagators at $t=10$ on a 20^4 lattice with $\beta=5.7$. (a) $m_q=0.01$, (b) $m_q=0.02$.

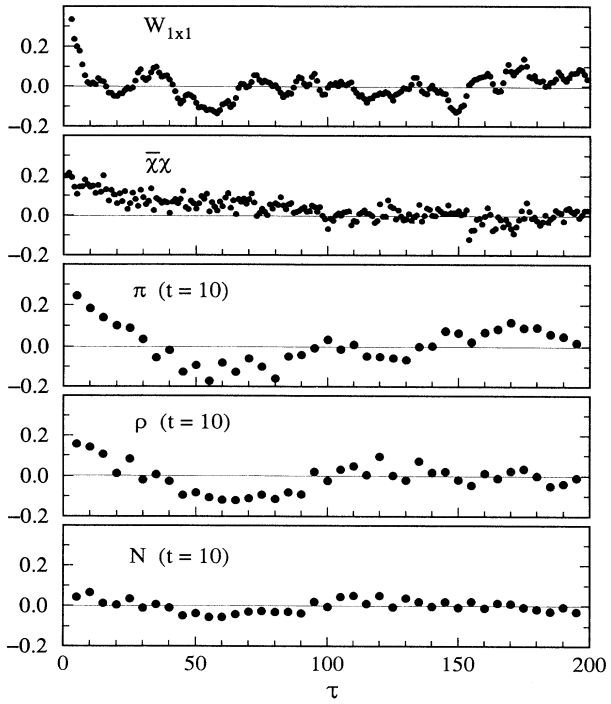

FIG. 5. Autocorrelation functions for 1×1 Wilson loop, chiral order parameter $\bar{\chi}\chi$, and $\pi(\gamma_5\xi_5)$, $\rho(\gamma_k\xi_k)$, and local nucleon (N) propagators at $t=10$ on a 20^4 lattice with $\beta=5.7$ and $m_q=0.01$.

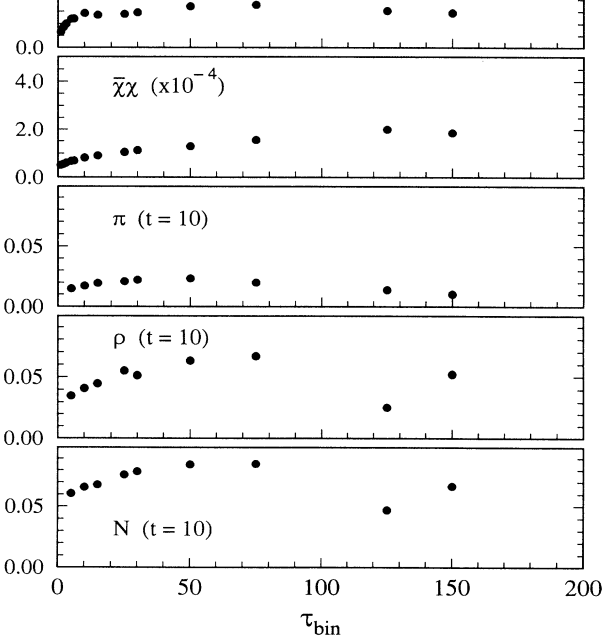

FIG. 6. Bin-size dependence of jack-knife error for the 1×1 Wilson loop, chiral order parameter $\bar{\chi}\chi$, and $\pi(\gamma_5\xi_5)$, $\rho(\gamma_k\xi_k)$, and local nucleon (N) propagators at $t=10$ on a 20^4 lattice with $\beta=5.7$ and $m_q=0.01$.

In Table IV we summarize the average values and errors of Wilson loops and the chiral order parameter for all of our runs.

III. HADRON MASS MEASUREMENT

A. Effective mass analysis

The hadron operators which are local in time carry a definite σ_s parity but create both $\sigma_t=+1$ and -1 states. The coupling of $\sigma_t=-1$ states has a sign factor $(-1)^t$ where t is the temporal separation between the source and the sink. We therefore expect hadron propagators to have the form

$$P(t)=A_+\{\exp(-m_+t)+(-1)^{\sigma_b\cdot t}\exp[-m_+(T-t)]\}+(-1)^tA_-\{\exp(-m_-t)+(-1)^{\sigma_b\cdot t}\exp[-m_-(T-t)]\}\ , \tag{3.1}$$

where m_+ and m_- denote the masses of states with the parity $P=+\sigma_s$ and $-\sigma_s$, and the second and the fourth terms represent contributions due to the periodic boundary condition with T the temporal lattice size and $\sigma_b=0$ and 1 for mesons and baryons.

Examples of our propagator data are shown in Fig. 7 for a $20^3\times(20\times2)$ lattice at $\beta=5.7$ with $m_q=0.01$. In these figures absolute values of propagators are plotted with positive and negative values distinguished by solid and open symbols. Solid curves represent the results of the fits to be described below. The oscillatory behavior in t expected from (3.1) is clearly observed. We also note that the contribution of the $P=+1$ state appears absent in the pion channel ($\sigma_s=+1$) shown in Fig. 7(a).

Extraction of hadron masses through fits of propagator data with the function (3.1) requires a careful choice of the fitting range to avoid contamination from higher excited states. In order to examine this problem we use the distance dependent effective mass $m_{\rm eff}(t)$, which is obtained by fitting four consecutive values of propagators at $t+i$ and their periodic reflections at $T-t-i$ for $i=0,1,2,3$ with (3.1). For the channels $\pi(\gamma_5\xi_5)$ and $\pi(\gamma_5\xi_3\xi_5)$ where we do not observe parity partners we extract $m_{\rm eff}(t)$ using a single hyperbolic cosine form.

The behavior of the effective mass $m_{\rm eff}(t)$ for some typical hadron states for a $20^3\times(20\times2)$ lattice at $\beta=5.7$ with $m_q=0.01$ are shown in Fig. 8. The errors are estimated by the jack-knife method ($\tau_{\rm bin}=50$). We observe that the effective mass for the pion $\pi(\gamma_5\xi_5)$ [Fig. 8(a)] reaches a plateau starting at $t\approx8$. A systematic wiggle as reported in Ref. [3], possibly due to a periodic multiplication of gauge configurations [31], is not apparent at least within our error of typically 1–2 %. This is illustrated in Fig. 9 where we replot Fig. 8(a) for the pion effective mass on an enlarged scale together with that of Ref. [3]. Compared to a 5% drop of the latter from $t\approx6$ to 10 which amounts to four standard deviations, we only observe a 1.4% decrease from $t\approx10$ to 14 which, furthermore, is comparable with the statistical error of 1–2 %.

TABLE IV. Average values of (a) chiral order parameter, (b) Wilson loops for $\beta=5.7$, and (c) Wilson loops for $\beta=5.6$, 5.5, and 5.4 for various lattice parameters. For averaging intervals see Table II. Errors are estimated by the jack-knife method with the bin size $\tau_{\rm bin}=50$ or 20 (for short runs with $\tau<500$ at $\beta<5.7$).

(a)

β	5.7		5.6		5.5		5.4
m_q	0.01	0.02	0.01	0.02	0.01	0.02	0.01
4^4	0.014 244(94)						0.020 51(48)
6^4	0.017 92(10)						0.055 3(49)
8^4			0.026 55(77)		0.041 6(22)		0.110 7(23)
$8^3\times16$	0.020 47(15)	0.040 36(31)					
10^4					0.054 5(23)		
12^4	0.025 76(64)	0.044 74(60)	0.033 95(99)				0.118 4(13)
16^4	0.028 21(34)	0.047 908(93)	0.039 93(28)	0.058 58(22)	0.060 35(60)	0.085 95(55)	
20^4	0.027 55(13)	0.048 52(14)					

(b)

β	5.7		5.7		5.7		5.7		5.7	5.7
	20^4		16^4		12^4		$8^3\times16$		6^4	4^4
m_q	0.01	0.02	0.01	0.02	0.01	0.02	0.01	0.02	0.01	0.01
1×1	0.577 323(34)	0.577 311(40)	0.577 19(10)	0.577 261(49)	0.577 292(82)	0.577 55(10)	0.577 70(13)	0.577 90(14)	0.578 23(23)	0.579 80(84)
1×2	0.364 836(49)	0.364 699(57)	0.364 65(13)	0.364 654(57)	0.364 77(12)	0.365 17(15)	0.377 98(18)	0.378 22(22)	0.366 42(30)	0.369 5(10)
1×3	0.235 544(48)	0.235 359(58)	0.235 39(12)	0.235 333(56)	0.235 48(12)	0.235 91(15)	0.239 63(17)	0.239 80(22)	0.237 42(29)	
1×4	0.152 875(43)	0.152 685(51)	0.152 76(10)	0.152 664(53)	0.152 82(11)	0.153 21(14)	0.154 89(14)	0.154 99(18)		
1×5	0.099 366(37)	0.099 189(43)	0.099 272(88)	0.099 170(45)	0.099 32(10)	0.099 66(11)				
1×6	0.064 612(31)	0.064 473(33)	0.064 558(67)	0.064 466(39)	0.064 582(87)	0.064 870(97)				
1×7	0.042 019(26)	0.041 908(25)	0.041 997(57)	0.041 934(32)						
1×8	0.027 333(23)	0.027 252(18)	0.027 323(56)	0.027 264(29)						
2×2	0.174 745(49)	0.174 475(59)	0.174 50(12)	0.174 498(83)	0.174 65(14)	0.175 13(17)	0.208 20(20)	0.208 48(25)	0.177 39(34)	0.183 6(10)
2×3	0.090 760(44)	0.090 467(50)	0.090 54(10)	0.090 560(82)	0.090 69(13)	0.091 12(14)	0.109 40(17)	0.109 55(22)	0.093 50(31)	
2×4	0.048 282(36)	0.048 038(40)	0.048 151(75)	0.048 116(70)	0.048 21(11)	0.048 57(10)	0.060 07(12)	0.060 20(17)		
2×5	0.025 888(26)	0.025 712(28)	0.025 750(59)	0.025 762(44)	0.025 821(87)	0.026 102(82)				
2×6	0.013 916(19)	0.013 803(18)	0.013 783(30)	0.013 839(42)	0.013 878(66)	0.014 062(59)				
2×7	0.007 493(12)	0.007 421(11)	0.007 388(42)	0.007 473(21)						
2×8	0.004 037 6(98)	0.004 001 4(78)	0.003 941(29)	0.004 031(26)						
3×3	0.041 018(33)	0.040 760(41)	0.040 854(78)	0.040 875(81)	0.040 95(11)	0.041 33(11)	0.045 77(13)	0.045 91(17)	0.043 83(25)	
3×4	0.019 471(23)	0.019 292(27)	0.019 383(65)	0.019 409(52)	0.019 469(80)	0.019 756(81)	0.022 058(90)	0.022 19(10)		
3×5	0.009 405(17)	0.009 294(17)	0.009 340(45)	0.009 349(42)	0.009 417(45)	0.009 592(55)				
3×6	0.004 577(12)	0.004 508(10)	0.004 537(30)	0.004 561(24)	0.004 568(35)	0.004 705(27)				
3×7	0.002 233(10)	0.002 190 5(69)	0.002 223(16)	0.002 225(17)						
3×8	0.001 086 8(61)	0.001 050 6(81)	0.001 053(23)	0.001 096(12)						
4×4	0.008 496(15)	0.008 371(21)	0.008 428(46)	0.008 456(34)	0.008 445(54)	0.008 687(66)	0.009 605(64)	0.009 781(70)		
4×5	0.003 813(11)	0.003 745(13)	0.003 793(30)	0.003 762(24)	0.003 788(42)	0.003 955(41)				
4×6	0.001 733 8(80)	0.001 688 7(85)	0.001 706(19)	0.001 735(15)	0.001 675(35)	0.001 823(31)				
4×7	0.000 790 2(79)	0.000 771 4(88)	0.000 754(25)	0.000 789(10)						

TABLE IV. (*Continued*).

(b)

β	5.7		5.7		5.7		5.7		5.7	5.7
	20^4		16^4		12^4		$8^3\times16$		6^4	4^4
m_q	0.01	0.02	0.01	0.02	0.01	0.02	0.01	0.02	0.01	0.01
4×8	0.000 366 7(84)	0.000 348 8(78)	0.000 318(22)	0.000 371(16)						
5×5	0.001 612 5(93)	0.001 563 6(96)	0.001 544(21)	0.001 572(20)	0.001 609(41)	0.001 685(32)				
5×6	0.000 697 5(72)	0.000 681 0(51)	0.000 655(15)	0.000 669(15)	0.000 689(21)	0.000 744(17)				
5×7	0.000 289 5(83)	0.000 287 5(87)	0.000 309(17)	0.000 275(16)						
5×8	0.000 125 6(54)	0.000 118 5(55)	0.000 106(15)	0.000 124(11)						
6×6	0.000 281 0(76)	0.000 281 6(81)	0.000 294(19)	0.000 273(18)	0.000 260(25)	0.000 309(35)				
6×7	0.000 116 9(88)	0.000 103 5(66)	0.000 096(21)	0.000 108 9(75)						
6×8	0.000 043 9(87)	0.000 046 0(72)	0.000 048(13)	0.000 045(21)						
7×7	0.000 038 5(78)	0.000 042 7(68)	0.000 038(22)	0.000 111(18)						
7×8	0.000 006 3(62)	0.000 011 4(93)	0.000 024(19)	0.000 018(25)						
8×8	0.000 010 7(67)	0.000 011(10)	−0.000 022(34)	0.000 051 4(76)						

(c)

β	5.6				5.5				5.4			
	16^4		12^4	8^4	16^4		10^4	8^4	12^4	8^4	6^4	4^4
m_q	0.01	0.02	0.01	0.01	0.01	0.02	0.01	0.01	0.01	0.01	0.01	0.01
1×1	0.565 02(14)	0.565 15(12)	0.565 36(14)	0.565 74(28)	0.550 02(19)	0.549 443(71)	0.551 04(36)	0.551 68(23)	0.529 43(23)	0.530 33(42)	0.535 72(72)	0.541 73(68)
1×2	0.349 06(15)	0.349 13(17)	0.349 74(20)	0.349 99(40)	0.329 92(26)	0.329 00(15)	0.331 42(57)	0.332 26(31)	0.303 50(31)	0.304 75(58)	0.312 4(10)	0.322 35(92)
1×3	0.220 24(14)	0.220 35(15)	0.221 09(20)	0.221 27(41)	0.202 07(24)	0.201 09(17)	0.203 63(60)	0.204 46(31)	0.177 27(31)	0.178 54(57)	0.186 14(98)	
1×4	0.139 67(14)	0.139 82(14)	0.140 54(20)	0.140 71(38)	0.124 41(21)	0.123 50(16)	0.125 72(54)	0.126 46(27)	0.103 95(26)	0.105 05(49)		
1×5	0.088 68(11)	0.088 80(13)	0.089 43(19)		0.076 70(19)	0.075 91(11)	0.077 77(46)		0.061 10(21)			
1×6	0.056 30(10)	0.056 49(11)	0.056 98(15)		0.047 31(15)	0.046 699(88)			0.035 92(15)			
1×7	0.035 752(79)	0.035 905(92)			0.029 176(87)	0.028 735(73)						
1×8	0.022 700(57)	0.022 812(63)			0.017 998(61)	0.017 652(72)						
2×2	0.159 59(13)	0.159 83(22)	0.160 50(22)	0.160 83(42)	0.141 81(26)	0.140 63(13)	0.143 20(65)	0.144 20(33)	0.117 19(35)	0.118 58(57)	0.126 9(10)	0.139 8(10)
2×3	0.079 095(90)	0.079 40(17)	0.080 01(17)	0.080 32(36)	0.066 14(20)	0.065 19(12)	0.067 25(50)	0.067 95(27)	0.048 89(23)	0.049 88(41)	0.056 28(83)	
2×4	0.040 117(85)	0.040 44(13)	0.040 92(12)	0.041 17(25)	0.031 69(13)	0.030 921(88)	0.032 39(37)	0.032 87(19)	0.020 79(16)	0.021 55(25)		
2×5	0.020 536(65)	0.020 746(98)	0.021 07(12)		0.015 26(11)	0.014 853(68)	0.015 74(29)		0.008 949(94)			
2×6	0.010 561(61)	0.010 667(74)	0.010 87(10)		0.007 403(68)	0.007 173(81)			0.003 940(61)			
2×7	0.005 442(34)	0.005 481(54)			0.003 560(40)	0.003 492(59)						
2×8	0.002 761(39)	0.002 780(27)			0.001 709(43)	0.001 646(38)						
3×3	0.033 388(69)	0.033 64(10)	0.034 08(16)	0.034 35(29)	0.025 49(16)	0.024 929(86)	0.026 23(33)	0.026 92(20)	0.015 89(15)	0.016 30(24)	0.020 62(53)	
3×4	0.014 810(61)	0.015 017(85)	0.015 41(14)	0.015 56(20)	0.010 403(96)	0.010 071(73)	0.010 68(24)	0.011 12(12)	0.005 43(10)	0.005 67(13)		
3×5	0.006 671(33)	0.006 882(89)	0.007 03(11)		0.004 345(76)	0.004 082(40)	0.004 40(16)		0.001 948(74)			
3×6	0.003 039(26)	0.003 050(53)	0.003 224(70)		0.001 826(22)	0.001 705(30)			0.000 704(67)			
3×7	0.001 339(33)	0.001 444(25)			0.000 711(48)	0.000 697(32)						
3×8	0.000 626(18)	0.000 696 6(91)			0.000 368(64)	0.000 351(28)						
4×4	0.005 946(52)	0.006 061(94)	0.006 212(85)	0.006 45(13)	0.003 794(75)	0.003 372(31)	0.003 66(18)	0.004 072(95)	0.001 471(51)	0.001 576(98)		
4×5	0.002 413(38)	0.002 484(57)	0.002 61(10)		0.001 424(49)	0.001 230(61)	0.001 333(87)		0.000 455(48)			
4×6	0.000 971(31)	0.001 083(44)	0.001 091(67)		0.000 496(75)	0.000 468(47)			0.000 069(45)			
4×7	0.000 429(31)	0.000 467(44)			0.000 187(29)	0.000 160(40)						

TABLE IV. (*Continued*).

(c)

β	5.6				5.5				5.4			
	16^4		12^4	8^4	16^4		10^4	8^4	12^4	8^4	6^4	4^4
m_q	0.01	0.02	0.01	0.01	0.01	0.02	0.01	0.01	0.01	0.01	0.01	0.01
4×8	0.000 216(31)	0.000 232(45)			0.000 030(19)	0.000 003(39)						
5×5	0.000 953(28)	0.000 912(77)	0.001 008(73)		0.000 460(29)	0.000 419(45)	0.000 374(72)		0.000 106(53)			
5×6	0.000 376(41)	0.000 372(10)	0.000 474(43)		0.000 184(56)	0.000 112(64)			0.000 054(34)			
5×7	0.000 164(27)	0.000 210(31)			0.000 051(59)	−0.000 010(41)						
5×8	0.000 061(20)	0.000 171(56)			0.000 022(24)	−0.000 051(33)						
6×6	0.000 194(34)	0.000 201(22)	0.000 187(55)		0.000 082(38)	0.000 042(61)			0.000 021(66)			
6×7	0.000 060(27)	0.000 019(32)			0.000 044(50)	0.000 053(57)						
6×8	−0.000 001(29)	0.000 045(38)			0.000 075(53)	−0.000 052(61)						
7×7	0.000 036(35)	0.000 088(26)			0.000 003(71)	−0.000 026(33)						
7×8	−0.000 003(36)	−0.000 026(59)			−0.000 038(43)	−0.000 032(53)						
8×8	0.000 087(33)	0.000 018(54)			0.000 020(61)	−0.000 008(61)						

Similar plateaus are observed from $t \approx 4$ for ρ [Figs. 8(b) and 8(c)] and $t \approx 6$ for the nucleon N [Fig. 8(e)]. For the particles $\sigma(J^{PC}=0^{++})$, $a_1(1^{++})$, $b_1(1^{+-})$, and Δ, the quality of data is worse, especially for b_1 and Δ for which we cannot see a plateau due to poor statistics. Combining these results with those of a similar analyses for other lattice sizes and parameters, we choose $T-t_{\min} \geq t \geq t_{\min}$ with $t_{\min}=8$ for the fitting range for the $\pi(\gamma_5\xi_5)$ channel and with $t_{\min}=6$ for other channels.

B. Fitting procedure

For extraction of hadron masses we make a global fit of propagator data to the function (3.1). For a $20^3\times(20\times2)$ lattice we minimize χ^2 defined by

$$\chi^2=\sum_{i,j=t_{\min}}^{T-t_{\min}}[\overline{P(i)}-P(i)](C^{-1})_{ij}[\overline{P(j)}-P(j)]\ , \tag{3.2}$$

where $\overline{P(i)}$ denotes a measured hadron propagator and the full covariance matrix C is given by

$$C_{ij}=\overline{P(i)P(j)}-\overline{P(i)}\ \overline{P(j)} \tag{3.3}$$

with the overline representing the ensemble average. For other cases the statistical quality of the covariance matrix is not sufficient and we evaluate χ^2 ignoring the off-diagonal elements of C.

Typical examples of fits with the full covariance matrix are illustrated in Fig. 7 for a $20^3\times(20\times2)$ lattice at $\beta=5.7$ with $m_q=0.01$ together with the fitted values of hadron masses and χ^2 per degree of freedom (the errors quoted are obtained by the jack-knife procedure as described below). Solid curves represent the absolute value of the functions given by

$$\begin{aligned}P_{\pm}(t)=&A_+\{\exp(-m_+t)+(\pm1)^{\sigma_b}\exp[-m_+(T-t)]\}\\&\pm A_-\{\exp(-m_-t)\\&\quad+(\pm1)^{\sigma_b}\exp[-m_-(T-t)]\}\ ,\end{aligned} \tag{3.4}$$

with $A_\pm$ and $m_\pm$ determined by the χ^2 fit. These curves should go through data points at even or odd values of t. We observe that the data are fitted nicely with reasonable values of χ^2 per degree of freedom. The relative magnitude of the two masses m_+ and m_- and the sign of the propagators are consistent with the particle assignment given in Table III.

We now consider the question of estimating errors of hadron masses. A standard procedure would be to study variations of fitted parameters under a unit increase of χ^2 from its minimum value. This requires reliable values for the covariance matrix C, which may be obtained by blocking the whole ensemble of configurations into statistically independent bins and taking averages in (3.3) over bin-averaged values of propagators. A practical problem with this procedure is that the number of bins has to be large, at least larger than the number of data points in order to make the covariance matrix nonsingular. For our $20^3\times(20\times2)$ lattice there are 40 data points, while our ensemble at $\beta=5.7$ with $m_q=0.01$ is divided into only 15 bins if we take the autocorrelation

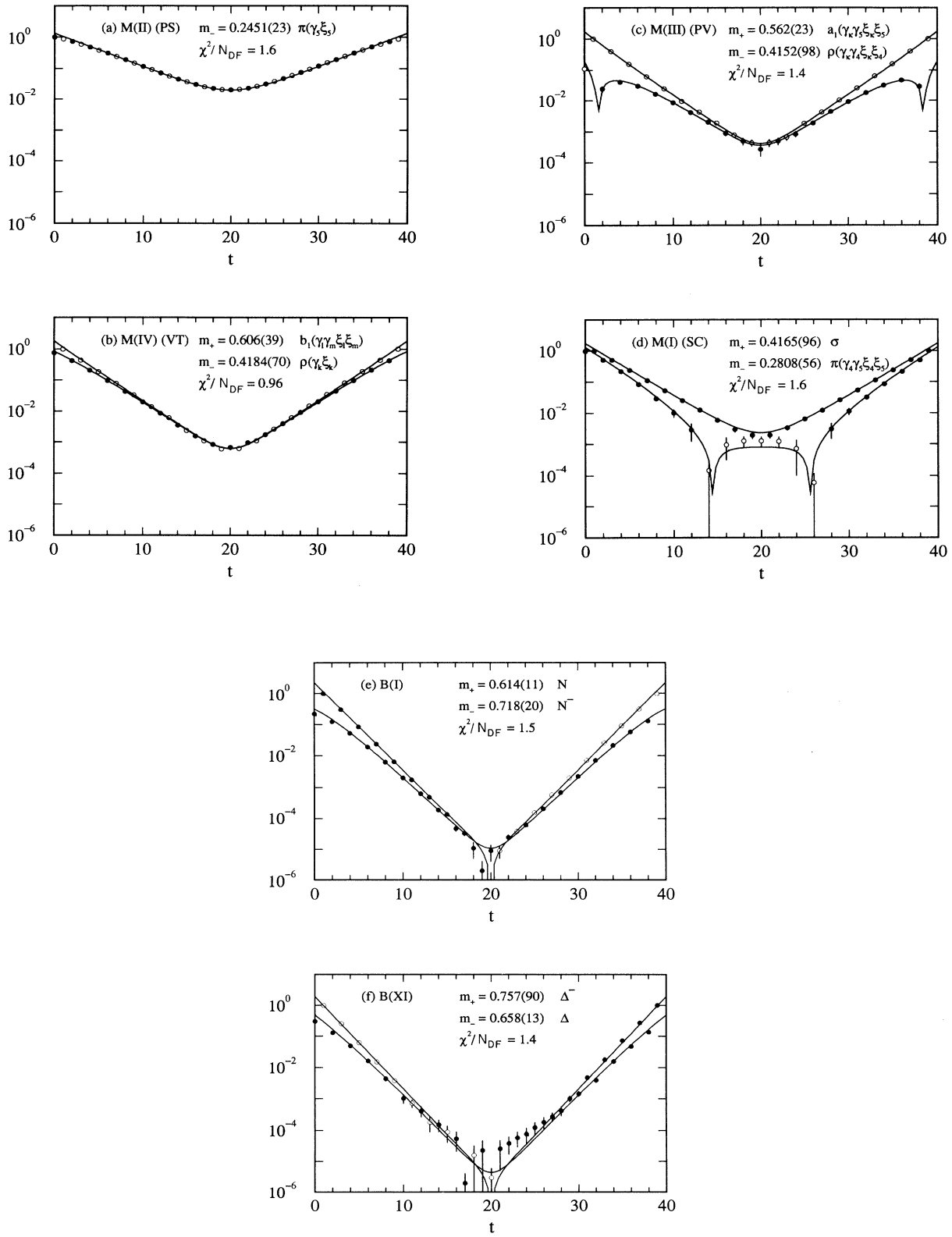

FIG. 7. Hadron propagators on a $20^3\times(20\times2)$ lattice with $\beta=5.7$ and $m_q=0.01$. See Table III for notation of operators. Absolute values of propagators are normalized to unity at $t=0$ or 1 for convenience. Solid and open symbols denote positive and negative values. Solid lines represent fits as described in text. The fitted values of masses and χ^2 per degree of freedom are also listed. Errors for masses are from jack-knife analysis with the bin size $\tau_{\rm bin}=50$.

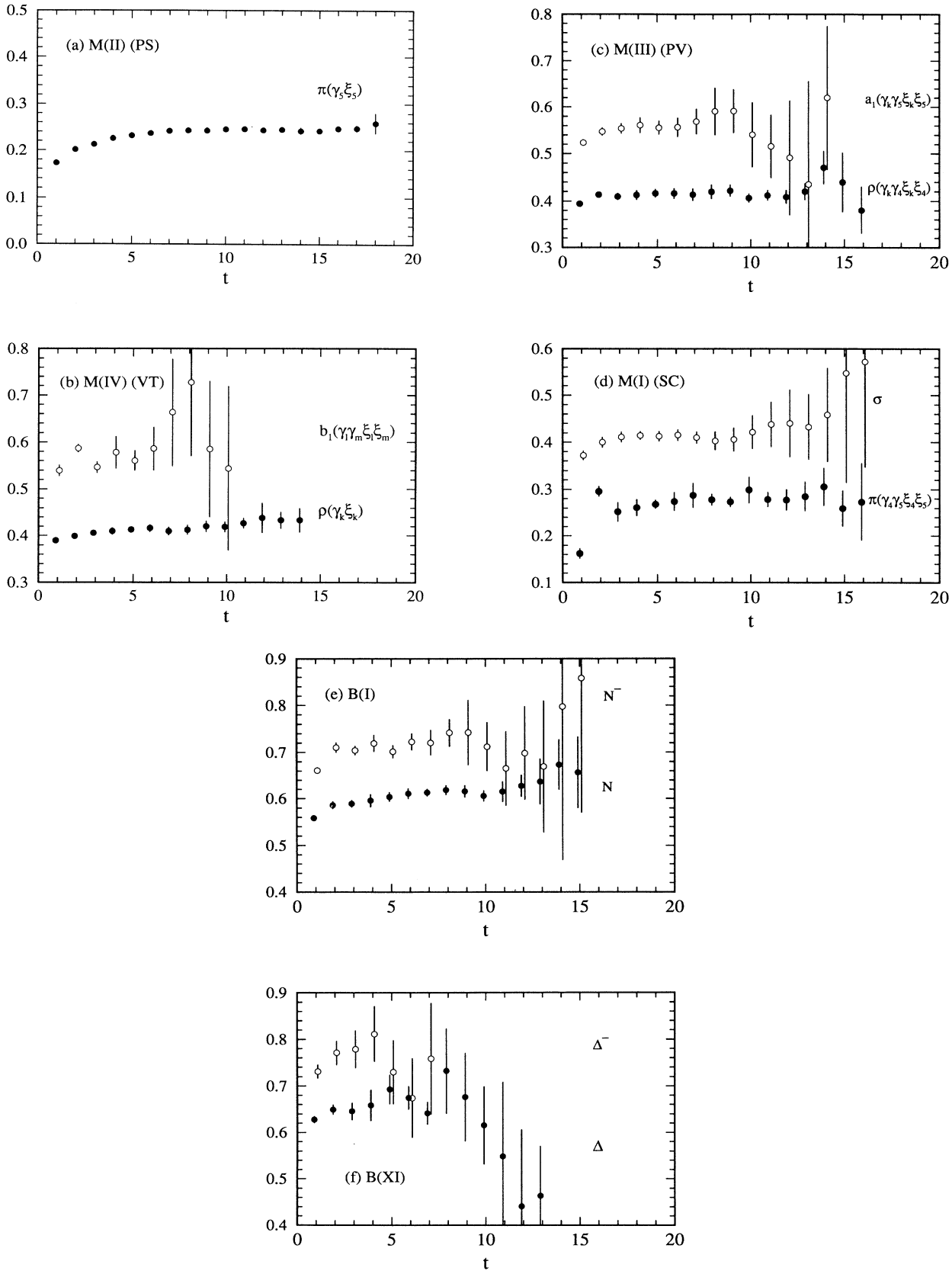

FIG. 8. Effective mass for the propagators shown in Fig. 7.

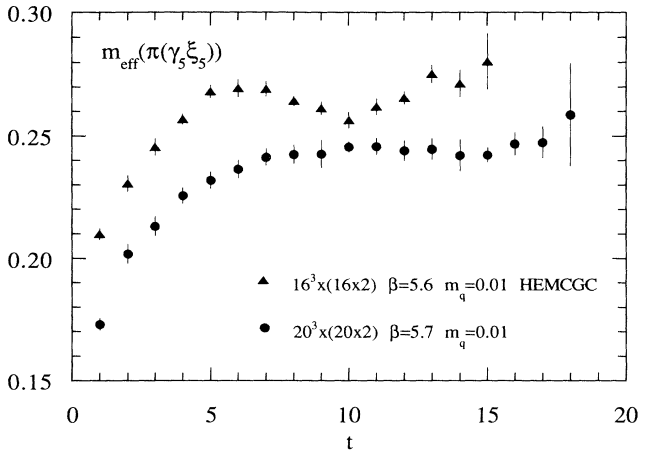

FIG. 9. Effective mass for $\pi(\gamma_5\xi_5)$ on a $20^3\times(20\times2)$ lattice at $\beta=5.7$ and $m_q=0.01$ plotted on an enlarged scale (circles). The data of the HEMCGC Collaboration [3] on an $16^3\times(16\times2)$ lattice at $\beta=5.6$ and $m_q=0.01$ is added for comparison (triangles).

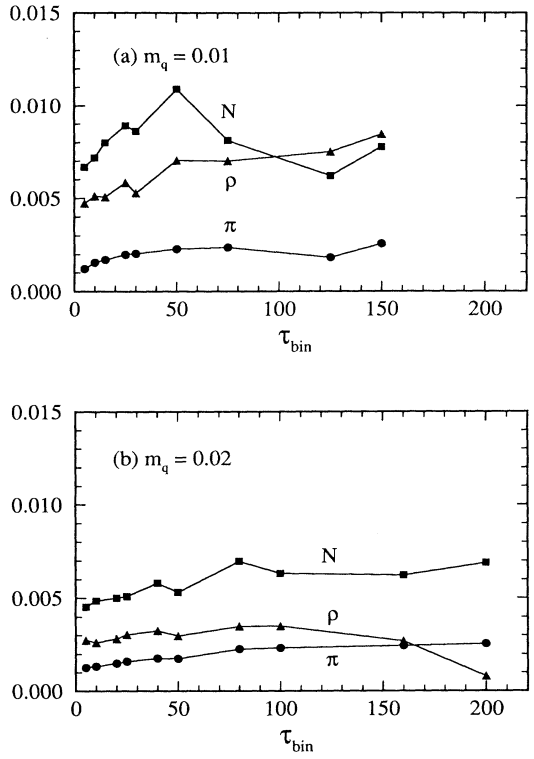

FIG. 10. Bin size dependence of jack-knife errors for $\pi(\gamma_5\xi_5)$, $\rho(\gamma_k\xi_k)$, and local nucleon (N) masses on a $20^3\times(20\times2)$ lattice with $\beta=5.7$ at (a) $m_q=0.01$ and (b) $m_q=0.02$.

time $\tau_{bin}\approx50$ as estimated in Sec. II E. Because of the severe demand of full QCD simulations on computing power, we cannot increase the number of bins easily. We therefore take an alternative approach: we remove configurations in one bin from the ensemble, construct hadron propagators and the covariance matrix using the remaining configurations, and make χ^2 fits. Repeating this procedure for each bin of the ensemble generates a set of masses which gives an estimate of error according to (2.20). A similar procedure is taken for lattices smaller than $20^3\times(20\times2)$ for which only diagonal elements of the covariance matrix are used for χ^2 fits [32].

The errors of hadron masses estimated in this way are shown in Fig. 10 as a function of the bin size τ_{bin} for π, ρ, and nucleon N. The magnitude of errors are almost saturated at $\tau_{bin}\approx50$. This is consistent with our estimate of the autocorrelation time for propagators made in Sec. II E.

C. Summary of mass results

Our results for hadron masses at $\beta=5.7$ for various lattice sizes are compiled in Table V (corresponding to the assignment in Table III). Errors are estimated by the jack-knife method with bin size $\tau_{bin}=50$. For the channels corresponding to $\rho(\gamma_k\xi_k)$ and $\rho(\gamma_k\gamma_4\xi_k\xi_4)$, propagators are averaged over $k=1-3$ before making global fits. For the number of configurations used see Table II.

The results for a $20^3\times(20\times2)$ lattice at $\beta=5.7$ are also shown in Fig. 11 where roman numerals below data points denote the operator names in Table III. Among the three pions $\pi(\gamma_5\xi_5)$, $\pi(\gamma_4\gamma_5\xi_4\xi_5)$, and $\pi(\gamma_5\xi_3\xi_5)$ the one corresponding to the Nambu-Goldstone pion $\pi(\gamma_5\xi_5)$ that couples to the operator M(II) is somewhat lighter ($\sim13\%$) than the two other pions (I and VII), which themselves are degenerate within errors. There are eight ρ mesons; two of them (XV_1 and XV_2) are members of the same $\mathbf{6}^+(\sigma_s=+1)$ representation, and the remaining six belong to different representations. All ρ masses are degenerate within errors of 1–2 %, showing a good restoration of flavor symmetry for this channel. The errors are quite large for $a_1(1^{++})$ and $b_1(1^{+-})$. No systematic deviation depending on the operators used is apparent beyond statistics, however.

For 11 baryon operators discussed in Sec. II D 1, 9 operators are assigned to the nucleon. The masses extracted from these operators are presented in Fig. 11(a) for $m_q=0.01$ and 11(b) for $m_q=0.02$. We observe that the masses for B(II), B(IV), $B(VII_1)$, B(VIII), B(IX), and $B(X_2)$ are consistent with the mass from the local nucleon operator B(I). We also expect that $B(VII_2)$ has a mass degenerate with $B(VII_1)$ as they are in the same **16** multiplet and $B(X_1)$ with $B(X_2)$ for the same reason. We see, however, that the masses of $B(VII_2)$ and $B(X_1)$ are significantly ($\sim10\%$) higher than those for the corresponding multiplet partners. The remaining two operators B(VI) and B(XI) belong to **8′** and are supposed to be Δ [20]. These masses are in fact about 10% larger than those for nucleons ($m_\Delta/m_N\approx1.12$ for $m_q=0.01$; ≈1.08 for $m_q=0.02$) in our simulation, supporting the assignment. It is interesting to note that the masses for $B(VII_2)$ and $B(X_1)$ are essentially those of Δ. It has been suggested that the first excited state which couples to operators in the **16** representation is the Δ baryon [20]. Our result may be understood if we assume that our wall sources

TABLE V. Hadron masses at $\beta=5.7$ with two flavors of dynamical KS fermions. Propagator is fitted for $t \geq 8$ for the M(II) channel with a single exponential and for $t \geq 6$ for other channels with two exponentials corresponding to $P=+1$ and -1 states. For the number of gauge configurations used see Table II. Errors are estimated by the jack-knife method with the bin size $\tau_{\rm bin}=50$.

		$20^3\times(20\times2)$		$16^3\times(16\times2)$		$12^3\times(12\times3)$		$8^3\times(16\times2)$	
	m_q	0.01	0.02	0.01	0.02	0.01	0.02	0.01	0.02
M(II) (PS)	$\pi(\gamma_5\xi_5)$	0.2451(23)	0.3403(17)	0.2552(38)	0.3326(34)	0.2963(95)	0.4115(99)	0.581(22)	0.609(17)
M(I) (SC)	$\pi(\gamma_4\gamma_5\xi_4\xi_5)$	0.2808(56)	0.3857(28)	0.251(16)	0.3735(52)		0.411(14)		
M(VII)	$\pi(\gamma_5\xi_3\xi_5)$	0.2839(32)	0.3822(21)	0.301(11)	0.3685(29)	0.348(11)	0.463(11)	0.655(23)	0.704(13)
M(III) (PV)	$\rho(\gamma_k\gamma_4\xi_k\xi_4)$	0.4152(98)	0.4991(34)	0.439(15)	0.4850(65)	0.486(22)	0.531(14)	0.676(70)	0.756(24)
M(IV) (VT)	$\rho(\gamma_k\xi_k)$	0.4184(70)	0.4916(30)	0.417(16)	0.4856(84)	0.500(29)	0.552(16)	0.711(42)	0.772(25)
M(VI)	$\rho(\gamma_1\gamma_4\xi_4)$	0.409(12)	0.4893(54)	0.511(22)	0.517(24)	0.519(75)	0.498(26)	0.635(58)	0.736(40)
M(X)	$\rho(\gamma_3\xi_2\xi_3)$	0.4217(81)	0.4890(24)	0.439(20)	0.461(14)	0.481(43)	0.586(30)	0.702(40)	0.780(29)
$M(\mathrm{XV}_1)$	$\rho(\gamma_2\xi_1)$	0.425(10)	0.4892(38)	0.407(25)	0.532(22)	0.468(25)	0.559(34)	0.704(59)	0.765(31)
$M(\mathrm{XV}_2)$	$\rho(\gamma_3\xi_2)$	0.4211(96)	0.4958(35)	0.393(18)	0.465(16)	0.480(48)	0.583(31)	0.702(40)	0.775(28)
M(XVI)	$\rho(\gamma_1\gamma_4\xi_3\xi_4)$	0.418(10)	0.4901(49)	0.486(12)	0.518(19)	0.519(79)	0.501(31)	0.605(65)	0.771(53)
M(XX)	$\rho(\gamma_2\xi_3\xi_1)$	0.4330(84)	0.4949(49)	0.445(18)	0.517(24)	0.463(23)	0.555(34)	0.674(60)	0.796(41)
M(I) (SC)	$\sigma(1)$	0.4165(96)	0.566(15)	0.374(66)	0.518(45)	0.387(11)	0.4867(60)	0.594(19)	0.649(10)
M(III) (PV)	$a_1(\gamma_k\gamma_5\xi_k\xi_5)$	0.562(23)	0.714(27)	0.483(80)	0.720(77)	0.577(35)	0.611(21)	0.704(40)	0.791(31)
M(VI)	$a_1(\gamma_1\gamma_5\xi_5)$	0.595(74)	0.766(77)	0.527(61)	0.496(42)	0.518(59)	0.606(35)	0.689(32)	0.801(36)
M(XVI)	$a_1(\gamma_1\gamma_5\xi_3\xi_5)$	0.584(76)	0.760(75)	0.367(27)	0.472(41)	0.538(60)	0.594(30)	0.689(40)	0.806(44)
M(IV) (VT)	$b_1(\gamma_l\gamma_m\xi_l\xi_m)$	0.606(39)	0.773(79)	0.55(14)	0.74(14)	0.530(69)	0.550(22)	0.695(79)	0.761(22)
M(X)	$b_1(\gamma_1\gamma_2\xi_1)$	0.594(88)	0.668(80)	0.63(17)	0.61(21)	0.475(63)	0.566(30)	0.687(41)	0.757(56)
$M(\mathrm{XV}_1)$	$b_1(\gamma_1\gamma_3\xi_2)$	0.613(64)	0.938(97)	0.27(16)	0.82(13)	0.47(13)	0.511(40)	0.664(73)	0.801(39)
$M(\mathrm{XV}_2)$	$b_1(\gamma_1\gamma_2\xi_1\xi_3)$	0.616(80)	0.650(63)	0.537(98)	0.59(12)	0.455(62)	0.573(33)	0.650(70)	0.726(46)
M(XX)	$b_1(\gamma_1\gamma_3\xi_2\xi_3)$	0.607(69)	0.842(72)	0.33(10)	0.65(14)	0.332(55)	0.556(47)	0.634(59)	0.826(56)
B(I)	N	0.614(11)	0.7359(53)	0.649(19)	0.734(12)	0.804(52)	0.929(21)	1.3580(41)	1.400(13)
B(II)	N	0.591(21)	0.7077(64)	0.771(72)	0.715(16)	0.731(39)	0.942(40)	1.37(14)	1.372(76)
B(IV)	N	0.605(12)	0.7143(67)	0.666(55)	0.707(20)	0.785(39)	0.913(33)	1.466(64)	1.305(58)
$B(\mathrm{VII}_1)$	N	0.636(20)	0.7258(95)	0.697(78)	0.744(20)	0.795(45)	0.956(29)	1.46(10)	1.42(13)
$B(\mathrm{VII}_2)$	N	0.73(11)	0.820(21)	0.31(29)	0.667(58)	2.9(1.0)	0.956(94)	1.37(58)	1.88(37)
B(VIII)	N	0.603(13)	0.7204(92)	0.665(46)	0.711(23)	0.769(73)	0.970(43)	1.52(14)	1.37(13)
B(IX)	N	0.606(19)	0.733(11)	0.67(12)	0.739(19)	0.73(13)	0.994(52)	1.33(21)	1.03(22)
$B(\mathrm{X}_1)$	N	0.679(27)	0.802(14)	0.84(16)	0.772(54)	0.728(63)	0.941(49)	1.40(16)	1.48(15)
$B(\mathrm{X}_2)$	N	0.624(15)	0.7377(86)	0.76(10)	0.719(23)	0.788(56)	0.970(30)	1.41(19)	1.68(45)
B(VI)	Δ	0.701(35)	0.811(18)	0.613(87)	0.853(61)	0.86(13)	1.128(76)	1.06(16)	1.32(35)
B(XI)	Δ	0.658(13)	0.803(17)	0.757(74)	0.775(38)	0.782(59)	1.072(62)	1.575(86)	1.36(10)

TABLE V. (*Continued*).

	m_q	$20^3\times(20\times2)$		$16^3\times(16\times2)$		$12^3\times(12\times3)$		$8^3\times(16\times2)$	
		0.01	0.02	0.01	0.02	0.01	0.02	0.01	0.02
B(I)	N^-	0.718(20)	0.949(27)	0.689(47)	0.879(35)	0.877(28)	0.964(24)	1.3586(35)	1.400(12)
B(II)	N^-	0.724(74)	1.38(19)	1.41(62)	0.74(12)	0.64(11)	1.083(72)	1.28(11)	1.33(12)
B(IV)	N^-	0.88(17)	0.99(14)	0.75(82)	0.82(14)	0.54(11)	1.00(12)	1.374(84)	1.30(13)
B(VII$_1$)	N^-	0.94(17)	0.85(10)	2.20(55)	0.76(15)	0.74(21)	0.950(51)	1.55(18)	1.15(16)
B(VII$_2$)	N^-	0.98(10)	0.98(10)	1.1(1.6)	0.96(24)	1.85(67)	0.97(10)	1.36(39)	1.08(23)
B(VIII)	N^-	0.604(87)	1.10(38)	0.50(14)	0.58(12)	1.15(45)	1.13(10)	1.32(32)	1.32(14)
B(IX)	N^-	0.77(16)	1.10(36)	2.57(74)	1.377(51)	1.3(1.1)	1.19(23)	1.67(43)	1.21(15)
B(X$_1$)	N^-	0.767(62)	1.06(13)	0.58(14)	0.833(60)	0.71(14)	1.014(63)	1.21(12)	1.31(23)
B(X$_2$)	N^-	0.750(45)	0.93(13)	2.50(31)	0.92(40)	0.49(11)	1.005(64)	1.20(18)	1.61(49)
B(VI)	Δ^-	0.90(12)	2.326(81)	0.41(44)	1.35(68)	0.93(22)	1.11(17)	2.83(63)	1.38(54)
B(XI)	Δ^-	0.757(90)	1.11(17)	0.86(32)	0.75(11)	0.86(20)	1.045(70)	1.20(13)	1.64(41)

emit Δ much more efficiently than the nucleon state for these operators [33].

At a fine level we also note that the central values of the nucleon masses differ appreciably more than for the case of the ρ meson. The fact that the pattern of variation is similar for $m_q=0.01$ and 0.02 suggests that this may not be merely due to statistics [34], but may rather be taken to be an operator dependence. The N-Δ mass splitting is an interesting quantity. The errors of the Δ mass, however, are sizable, and we need much more statistics for a quantitative estimate of the N-Δ mass splitting.

We have only limited statistics for $\beta<5.7$. For completeness we list the results for hadron masses obtained for local operators in Table VI. The bin size for jackknife error analyses is $\tau_{\rm bin}=20$ for this table due to the shortness of runs.

D. Determination of physical scale

The physical scale of the lattice spacing is the basic parameter which is estimated from hadron mass measurements. To estimate its value at $\beta=5.7$, we extrapolate the mass data for our largest spatial lattice size $L=20$ toward small quark masses assuming that

$$m_\pi^2 = A_\pi m_q + B_\pi \tag{3.5}$$

for the pion and

$$m_H = A_H m_q + B_H \tag{3.6}$$

for other hadrons. The values of parameters A and B are

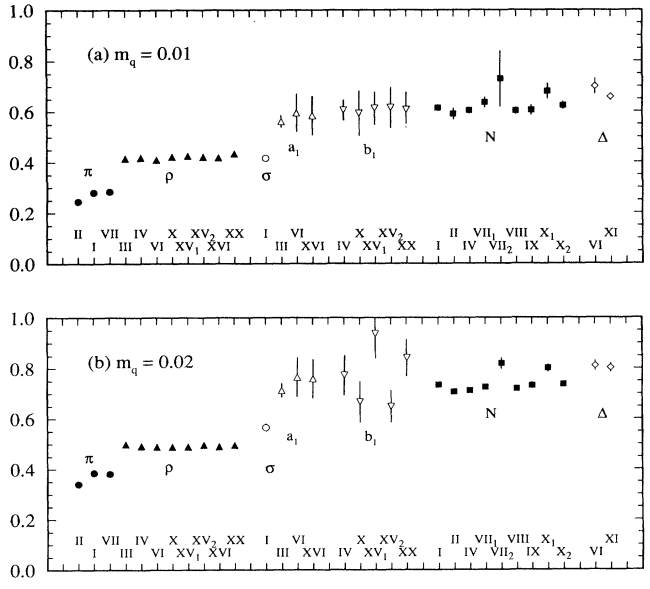

FIG. 11. Hadron mass spectrum for two dynamical flavors of KS fermions on a $20^3\times(20\times2)$ lattice at $\beta=5.7$ with (a) $m_q=0.01$ and (b) $m_q=0.02$. Roman numerals below data points denote operators used to extract the masses (see Table III).

TABLE VI. Hadron masses for local operators at $\beta=5.6$ and 5.5 with two flavors of dynamical KS fermions. For the number of gauge configurations used see Table II. Errors are estimated by the jack-knife method with the bin size $\tau_{\rm bin}=20$.

	β	5.6			5.5		
		$16^3\times(16\times2)$		$12^3\times(12\times3)$	$16^3\times(16\times2)$		$10^3\times(10\times3)$
	m_q	0.01	0.02	0.01	0.01	0.02	0.01
M(II) (PS)	$\pi(\gamma_5\xi_5)$	0.2648(47)	0.3696(31)	0.2528(81)	0.2942(44)	0.3901(17)	0.3148(65)
M(I) (SC)	$\pi(\gamma_4\gamma_5\xi_4\xi_5)$	0.535(89)	0.446(14)		0.40(10)	0.656(33)	0.71(28)
M(III) (PV)	$\rho(\gamma_k\gamma_4\xi_k\xi_4)$	0.488(49)	0.556(29)	0.483(73)	0.734(89)	0.759(28)	0.61(18)
M(IV) (VT)	$\rho(\gamma_k\xi_k)$	0.560(32)	0.563(11)	0.417(41)	0.636(37)	0.758(48)	0.686(83)
M(I) (SC)	$\sigma(1)$	1.01(49)	0.57(17)	0.311(32)	0.35(10)	0.91(12)	0.547(91)
M(III) (PV)	$a_1(\gamma_k\gamma_5\xi_k\xi_5)$	0.87(94)	1.22(25)	0.60(15)	1.8(1.3)	1.04(40)	0.42(86)
M(IV) (VT)	$b_1(\gamma_l\gamma_m\xi_l\xi_m)$	1.53(83)	2.07(62)	0.59(26)	0.94(68)	3.0(1.6)	0.88(88)
B(I)	N	0.725(68)	0.84(10)	0.721(42)	0.999(82)	1.149(51)	1.10(17)
B(I)	N^-	1.0(1.6)	0.78(64)	0.742(96)	1.43(57)	0.920(75)	1.41(22)

TABLE VII. Coefficients for linear extrapolation $m_\pi^2=A_\pi m_q+B_\pi$ for pions and $m_H=A_H m_q+B_H$ for other hadrons as a function of the quark mass at $\beta=5.7$. Result for the chiral order parameter is also given.

	$20^3\times(20\times2)$		$16^3\times(16\times2)$		$12^3\times(12\times3)$		$8^3\times(16\times2)$	
	A	B	A	B	A	B	A	B
$\pi(\gamma_5\xi_5)$ (PS)	5.57(16)	0.0043(25)	4.55(30)	0.0197(45)	8.15(99)	0.006(14)	3.3(3.3)	0.305(55)
$\pi(\gamma_4\gamma_5\xi_4\xi_5)$ (SC)	6.99(38)	0.0090(67)	7.64(89)	−0.012(17)				
$\pi(\gamma_5\xi_3\xi_5)$	6.55(24)	0.0151(39)	4.49(67)	0.046(13)	9.3(1.3)	0.028(18)	6.6(3.4)	0.363(62)
$\rho(\gamma_k\gamma_4\xi_k\xi_4)$ (PV)	8.4(1.0)	0.331(20)	4.6(1.6)	0.394(31)	4.5(2.6)	0.441(45)	8.0(7.4)	0.60(14)
$\rho(\gamma_k\xi_k)$ (VT)	7.32(76)	0.345(14)	6.9(1.8)	0.348(33)	5.2(3.3)	0.448(61)	6.1(4.9)	0.651(87)
$\sigma(1)$ (SC)	14.9(1.8)	0.267(24)	14.4(8.0)	0.23(14)	10.0(1.3)	0.286(24)	5.5(2.1)	0.539(39)
$a_1(\gamma_k\gamma_5\xi_k\xi_5)$ (PV)	15.2(3.5)	0.411(53)	24(11)	0.25(18)	3.4(4.1)	0.543(74)	8.6(5.0)	0.618(85)
$b_1(\gamma_l\gamma_m\xi_l\xi_m)$ (VT)	16.7(8.8)	0.44(11)	18(20)	0.37(32)	2.1(7.2)	0.51(14)	6.6(8.2)	0.63(16)
N(I)	12.2(1.2)	0.492(22)	8.5(2.3)	0.564(41)	12.5(5.6)	0.68(11)	4.2(1.3)	1.316(15)
Δ(XI)	14.5(2.1)	0.512(31)	1.8(8.3)	0.74(15)	29.0(8.6)	0.49(13)	2.1(13)	1.79(20)
$\langle\bar{\chi}\chi\rangle$	2.097(19)	0.006 58(30)	1.969(35)	0.008 51(68)	1.898(88)	0.0068(14)	1.989(34)	0.000 58(43)

tabulated in Table VII. The extrapolation is illustrated in Fig. 12 for $\pi(\gamma_5\xi_5)$, $\rho(\gamma_k\xi_k)$, N(I) and Δ(XI). For the pion B_π is quite close to zero, consistent with spontaneous breakdown of chiral symmetry. For local nucleon, we obtain $m_N/m_\rho|_{m_q=0}=B_N/B_\rho=1.426(86)$ using $\rho(\gamma_k\xi_k)$ and 1.49(11) with $\rho(\gamma_k\gamma_4\xi_k\xi_4)$, as compared with 1.221(experiment). Statistics is too poor for a reliable estimate of a_1 and b_1 masses: our analysis suggests that they are placed around the nucleon mass, appreciably lower than the empirical values.

The inverse lattice spacing a^{-1} can be estimated from the intercept B_H at $m_q=0$ and the experimental value of the mass of hadron H. The result obtained with $m_\rho=770$ MeV as input is $a^{-1}=2.23(9)$ GeV for the local $\rho(\gamma_k\xi_k)$ meson and 2.33(14) GeV for $\rho(\gamma_k\gamma_4\xi_k\xi_4)$, and with $m_N=940$ MeV we find $a^{-1}=1.91(9)$ GeV for the local nucleon mass. These values are tabulated in Table VIII. Also listed in the table are the corresponding values of the QCD scale parameter Λ_L and $\Lambda_{\overline{\rm MS}}$ for $N_f=2$, which are related by $\Lambda_{\overline{\rm MS}}/\Lambda_L=43.88$ [35], where $\overline{\rm MS}$ denotes the modified minimal subtraction scheme. The 15% discrepancy in the scales determined from the ρ and nucleon masses reflect the uncertainty due to finite-size as well as finite-lattice-spacing effects. We shall discuss finite-size effects in Sec. IV.

In order to see finite-lattice-spacing effects we compare in Fig. 13 our result for the inverse lattice spacing a^{-1} at $\beta=5.7$ with the values determined from $\rho(\gamma_k\xi_k)$ and local nucleon masses in the previous simulations with two flavors of dynamical Kogut-Susskind fermions [2–4] (we do not use our data for $\beta<5.7$ because of poor statistics). We observe a trend that the difference between the two sets of values diminishes as β increases. The solid lines in Fig. 13 represent the behavior of a^{-1} expected from two-loop asymptotic scaling with the value $\Lambda_{\overline{\rm MS}}=200$ MeV and 150 MeV. The lattice results over the range $\beta=5.3-5.7$ are smaller than the two curves. They show,

TABLE VIII. Physical scale for full QCD with two dynamical flavors of KS fermions at $\beta=5.7$ obtained on a $20^3\times(20\times2)$ lattice using local ρ and nucleon masses at $m_q=0$. $m_\rho=770$ MeV or $m_N=940$ MeV is used as input.

	$m_\rho=770$ MeV		$m_N=940$ MeV
	$\rho(\gamma_k\xi_k)$	$\rho(\gamma_k\gamma_4\xi_k\xi_4)$	N
a^{-1} (GeV)	2.23(9)	2.33(14)	1.91(9)
Λ_L (MeV)	2.91(12)	3.04(18)	2.49(11)
$\Lambda_{\overline{\rm MS}}$ (MeV)	127(5)	133(8)	109(5)
$m_q(a)$ (MeV)	1.58(8)	1.51(10)	1.84(10)
$m_q(\mu=1$ GeV) (MeV)	2.20(11)	2.10(14)	2.55(14)

however, an increase with β which is faster than the asymptotic scaling. It seems likely that a^{-1} rises up to values corresponding to $\Lambda_{\overline{\rm MS}}\approx150-200$ MeV for larger β.

Another interesting quantity is the value of quark mass in physical units. For the bare quark mass $m_q(a)$ at a lattice cutoff $1/a$ this may be estimated by $m_q(a)=(m_\pi a)^2/(A_\pi a)$ with $m_\pi=140$ MeV (see Table VIII). Relating the bare value to the renormalized quark mass $m_q(\mu)$ at some scale μ requires a perturbative calculation of quark self-energy for Kogut-Susskind fermions. The one-loop result [36] is

$$m_q(\mu)=m_q(a)\left[1-\frac{4}{3}g^2\left[\frac{3}{8\pi^2}\ln a\mu-\sigma_S+\tau+z_S\right]\right] \tag{3.7}$$

with $\sigma_S=0.19745(3)$, $\tau=-0.044566(13)$, and $z_S=-1/(16\pi^2)$ for the $\overline{\rm MS}$ scheme. The one-loop correction is positive and not small numerically. For $\mu=1$ GeV we find $m_q(\mu)/m_q(a)=1+0.3718g^2=1.39$ at $\beta=6/g^2=5.7$ with $a^{-1}=2.23$ GeV as determined by the mass of $\rho(\gamma_k\xi_k)$, and hence the renormalized quark mass

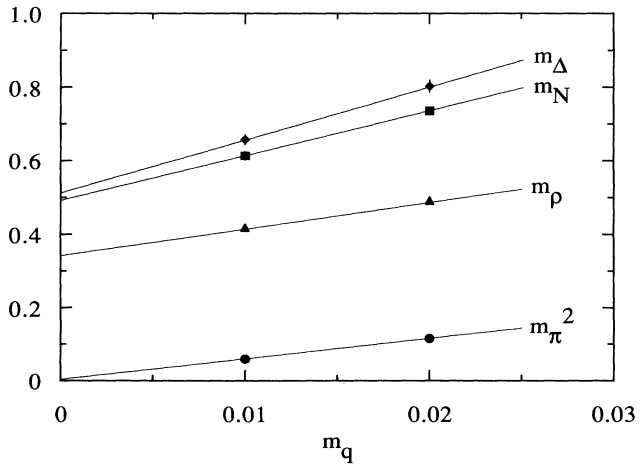

FIG. 12. Quark mass dependence of $\pi(\gamma_5\xi_5)$, $\rho(\gamma_k\xi_k)$, local nucleon (N) and Δ [B(XI)] masses. For the pion, mass squared is plotted. Solid lines are linear extrapolation to $m_q=0$.

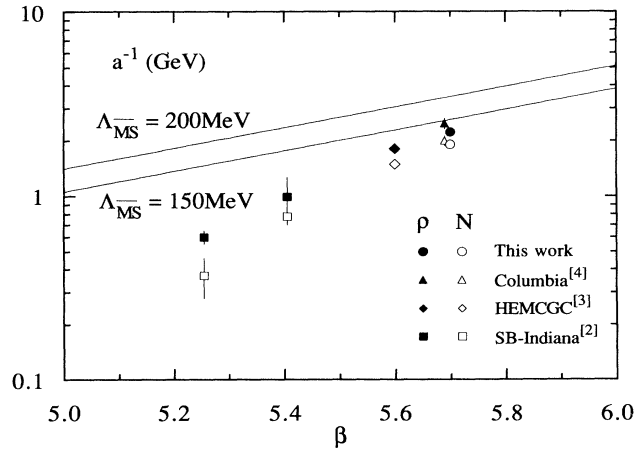

FIG. 13. Inverse lattice spacing in GeV units as determined from $\rho(\gamma_k\xi_k)$ (solid symbols) and local nucleon (open symbols) masses for two flavors of KS fermions. Solid lines represent two-loop asymptotic scaling with $\Lambda_{\overline{\rm MS}}=200$ and 150 MeV.

at $\mu=1$ GeV is estimated as $m_q(\mu=1\ \text{GeV})=2.2$ MeV. (The results for other determinations of a^{-1} are similar. See Table VIII.) This value is quite small compared to the estimate $(m_u+m_d)/2\approx 6-7$ MeV ($\mu=1$ GeV) deduced by QCD sum rules and current algebra (see, e.g., Ref. [37]).

In Fig. 14(a) we have compiled the renormalized quark mass at 1 GeV in the $\overline{\text{MS}}$ scheme obtained in the quenched and two-flavor full QCD simulations with the Kogut-Susskind fermion action using $\rho(\gamma_k\xi_k)$ to fix the scale. We see that a reasonable agreement between the quark mass derived from two-flavor simulations ($m_q\approx 7$ MeV) and its empirical value, as observed at $\beta\approx 5.25$, is lost as β increases; the quark mass from the simulations decreases rapidly with an increasing β. The same trend is also seen for the quenched ($N_f=0$) case. In fact a shift of $\delta\beta\approx 0.3$, which roughly matches the lattice spacing for $N_f=0$ and for $N_f=2$ cases, makes the quark mass for the two cases almost identical.

For comparison we present in Fig. 14(b) the renormalized quark mass with the Wilson action. We used the definition $m_q(a)=(K^{-1}-K_c^{-1})/2a$ for the bare quark mass and the one-loop correction is given by [38]

$$m_q(\mu)=m_q(a)\left[1-\frac{g^2}{2\pi^2}(\ln a\mu-2.15)\right]. \tag{3.8}$$

We see that the quark mass for $N_f=2$ exhibits only a small change as β increases and stays for $\beta=5.4-5.6$ at $m_q\approx 2$ MeV, a value a factor of 3 smaller than is inferred phenomenologically. In contrast with the case for the Kogut-Susskind action, the quark mass from the quenched simulations is about a factor 2 larger than the full QCD value even after the shift of the coupling constant $\delta\beta\approx 0.3$ that matches the lattice spacing of the two cases.

It has often been stated that the Kogut-Susskind and Wilson formalisms yield consistent results for observable quantities. This statement does not seem to apply to the case with the mass of quarks, at least so far as we take the

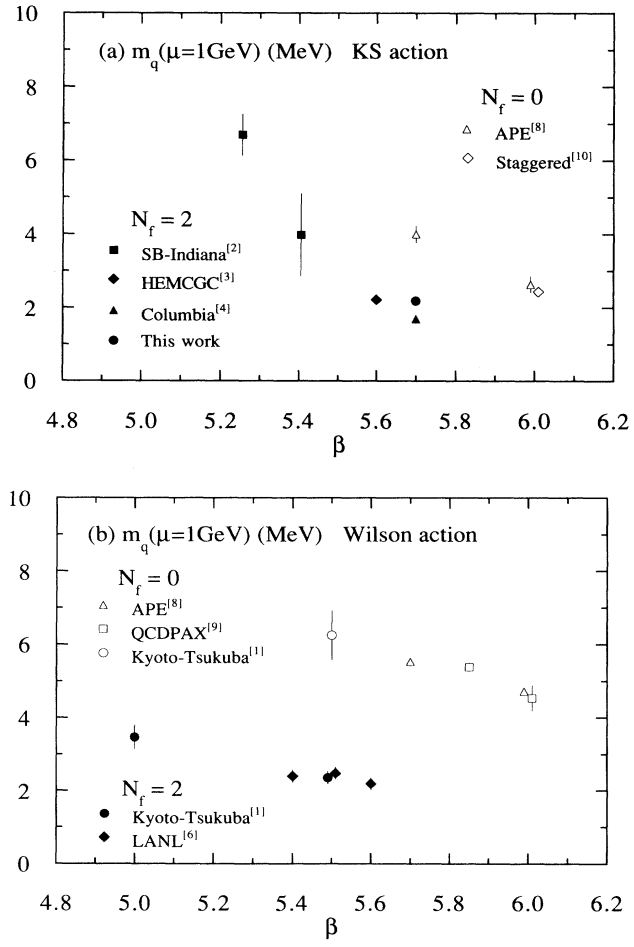

FIG. 14. Renormalized quark mass at $\mu=1$ GeV in full QCD with two flavors of dynamical quarks (solid symbols) and in the quenched approximation (open symbols). (a) KS fermion action, (b) Wilson action.

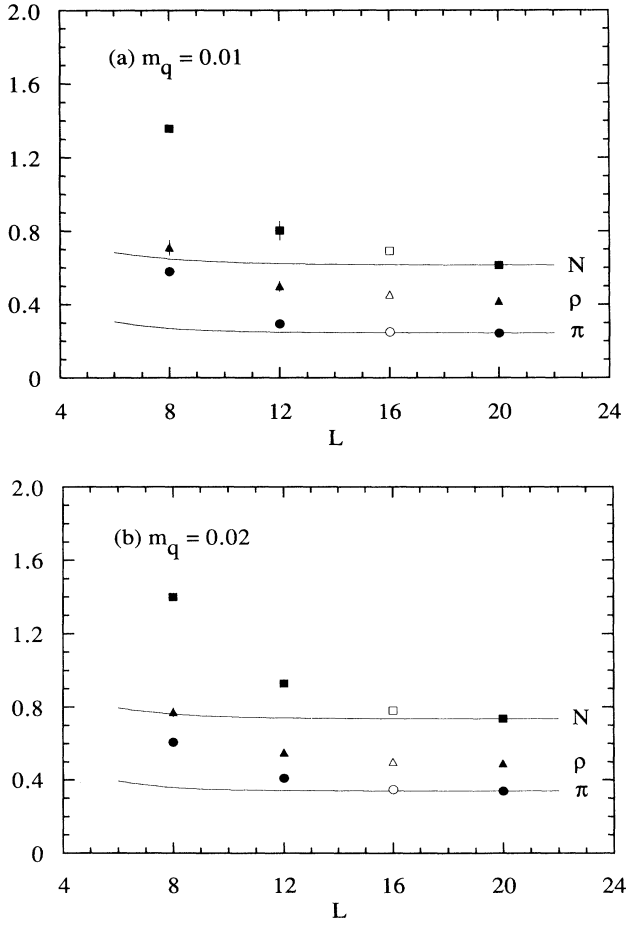

FIG. 15. Dependence of $\pi(\gamma_5\xi_5)$, $\rho(\gamma_k\xi_k)$, and local nucleon (N) masses on the spatial lattice size L. Solid lines are predictions of analytic formula for the size effect due to virtual pion emission [see (4.2)–(4.3)]. Open symbols at $L=16$ are the data of the Columbia group [4]. (a) $m_q=0.01$, (b) $m_q=0.02$.

conventional definition of the quark mass for the two actions.

IV. FINITE-SIZE EFFECTS IN HADRON MASSES

A. Lattice-size dependence of hadron mass data

Finite-lattice-size effects are one of the main sources of systematic errors in a numerical determination of the hadron mass spectrum. In order to study this problem in detail we have carried out mass measurements for the spatial lattice sizes $L=8$, 12, 16, and 20 at $\beta=5.7$. We concentrate on the size dependence of $\pi(\gamma_5\xi_5)$, $\rho(\gamma_k\xi_k)$ and nucleon masses extracted from local operators since they have the best statistical quality in our mass data. For the spatial lattice size $L=16$ we adopt the data of the Columbia group [4] which are based on ten times more statistics than our short runs.

In Fig. 15 m_π, m_ρ, and m_N at $\beta=5.7$ are plotted as a function of the spatial lattice size L for $m_q=0.01$ and 0.02. We see a steep decrease of all these masses for the lattice sizes $L=8-16$. For $m_q=0.01$ the size dependence is quite significant even from $L=16$ to $L=20$; the pion mass drops by 2.7% (three standard deviations), the ρ mass by 8% (five standard deviations), and more conspicuously the nucleon mass decrease by 11% which amounts to seven standard deviations. The magnitude of the size-dependent shift is smaller for a heavier quark mass of $m_q=0.02$: the difference between $L=16$ and 20 is 2.5% for m_π, 2% for m_ρ, and the decrease of m_N reduces to a level of 6%.

An increase of the size effect for smaller quark masses can be seen in a different way. Figure 16 compares the quark mass dependence of m_π^2, m_ρ, and m_N obtained for $L=16$ [4] and 20 spatial sizes. The discrepancy between the data for $L=16$ and those for $L=20$ is apparent for small quark mass, especially for ρ and the nucleon. It should be noted that the masses for $L=16$ at $m_q=0.01$ are shifted significantly upwards compared to the linear extrapolation of data for higher quark masses, whereas those for $L=20$ are consistent with the extrapolation.

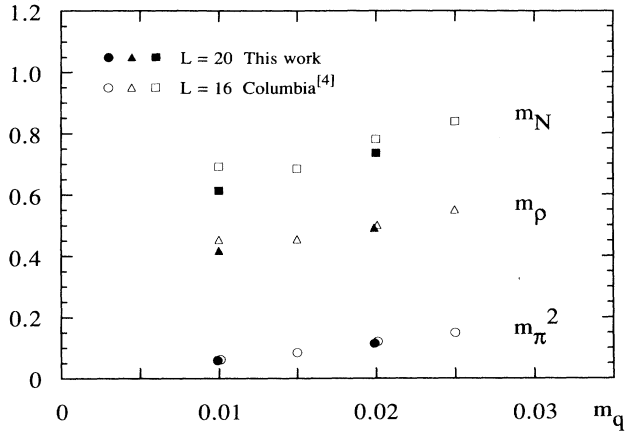

FIG. 16. Comparison of hadron masses for spatial size $L=16$ [4] (open symbols) and $L=20$ (solid symbols) as functions of the quark mass.

B. Origin of size effects

We may think of three possible sources of finite-size effects observed in Fig. 15: propagation of virtual pions around the lattice, extent of hadron wave functions relative to the lattice size, and restoration of chiral symmetry for small lattice volumes.

The effect of virtual particles on particle masses in a finite spatial box has been extensively studied by analytic methods [14,15]. In a ϕ^4 scalar field theory, for example, the one-loop perturbative contribution to mass renormalization is proportional to $\Delta(\mathbf{0},0)$ where $\Delta(\mathbf{x},t)$ is the free propagator. On a finite spatial box of a size L^3 with the periodic boundary condition this expression is modified to $\sum_{l\in\mathbb{Z}^3}\Delta(lL,0)$ where the terms with $l\neq\mathbf{0}$ represent the effect of a virtual particle propagating around the box. These terms give rise to an L-dependent shift in the mass of the form $\exp(-cmL)$. Generalization to all orders of perturbation theory leads to the asymptotic formula [14] for the mass $m(L)$ on a box of a size L^3:

$$m(L)-m=-\frac{3}{16\pi m^2 L}\left[\lambda^2\exp\left[-\frac{\sqrt{3}}{2}mL\right]+\frac{m}{\pi}\int_{-\infty}^{\infty}dy\,e^{-\sqrt{m^2+y^2}L}F(iy)+O(e^{-\bar{m}L})\right], \tag{4.1}$$

where $m=m(\infty)$, λ denotes the three-point coupling constant and $F(\nu)$ is the forward elastic scattering amplitude with $\nu=(s-u)/4m$ the crossing variable. The last term $O(e^{-\bar{m}L})$ damps faster than the other terms (e.g., $\bar{m}\geq\sqrt{3/2}m$).

Applying the general formula (4.1) one can estimate the sign and magnitude of the finite-size shift for hadrons [14]. For the pion the three-point coupling is absent. Substituting the current algebra result $F(\nu)=-m_\pi^2/f_\pi^2+O(\nu^2,m_\pi^4)$, one finds

$$\frac{m_\pi(L)-m_\pi}{m_\pi}=\frac{3}{8\pi^2}\frac{m_\pi^2}{f_\pi^2}\frac{1}{m_\pi L}K_1(m_\pi L)\underset{L\to\infty}{\sim}\frac{3}{8\sqrt{2}\pi^{3/2}}\frac{m_\pi^2}{f_\pi^2}\frac{1}{(m_\pi L)^{3/2}}e^{-m_\pi L}, \tag{4.2}$$

where $K_1(z)$ is the modified Bessel function. The positive sign of the size effect predicted by (4.2) is consistent with our numerical result. However, the magnitude is far too small, as illustrated by the solid line in Fig. 15, for which we used the measured value of the pion mass obtained on a $20^3\times(20\times2)$ lattice for m_π and $f_\pi=0.0421$ for the pion decay constant (see Sec. V C). To quote numerical values, (4.2) gives $[m_\pi(L)-m_\pi]/m_\pi=1.9\%$ ($L=12$) and 0.45% ($L=16$) at $m_q=0.01$ as compared to 21% ($L=12$) and 2.8% ($L=16$) for the simulation data.

A similar analysis can be carried out for the nucleon mass. In this case the three-point coupling is given by $\lambda=ig_{\pi NN}$

with $g^2_{\pi NN}/4\pi \approx 14.3$ the pion nucleon coupling constant, and one finds that [14]

$$\frac{m_N(L)-m_N}{m_N}=\frac{9}{4}\left[\frac{m_\pi}{m_N}\right]^3\frac{g^2_{\pi NN}}{4\pi}\frac{1}{m_\pi L}e^{-\sqrt{1-v_B^2/m_\pi^2}\,m_\pi L}-\frac{3}{16\pi^2}\left[\frac{m_\pi}{m_N}\right]^2\int_{-\infty}^{+\infty}dp\,e^{-m_\pi L\sqrt{1+p^2}}F_{\pi N}(im_\pi p)\,, \tag{4.3}$$

where $v_B=m_\pi^2/2m_N$ and $F_{\pi N}(\nu)=6m_N[A^{(+)}(\nu)+\nu B^{(+)}(\nu)]$ with $A^{(+)}$ and $B^{(+)}$ the conventional crossing-even pion-nucleon forward scattering amplitudes. To estimate the magnitude of (4.3) it is convenient to separate out the nucleon pole contribution to $F_{\pi N}(\nu)$,

$$F_{\pi N}(\nu)=\frac{6g^2_{\pi NN}}{1-(\nu/\nu_B)^2}+\bar{F}_{\pi N}(\nu)\,, \tag{4.4}$$

and use the parametrization

$$\bar{F}_{\pi N}(\nu)=\sum_{k=0}^{\infty}r_k(\nu/m_\pi)^{2k},\quad |\nu|<m_\pi\,, \tag{4.5}$$

with $r_0=-60.7$, $r_1=45.3$, and $r_2=8.1$ determined from the πN dispersion analyses [39]. Substituting the values $m_N=0.614$ and $m_\pi=0.2451$ found on a $20^3\times(20\times2)$ lattice and integrating the nonpole term (4.5) over $|\nu|\le m_\pi$ one obtains the curve in Fig. 15. The size effect is positive also for the nucleon mass, but the magnitude is quite small, comparable to that for the pion. This is quite different from the pattern observed in Fig. 15 which shows a much larger size effect for the nucleon than for the pion. Numerically we find $[m_N(L)-m_N]/m_N=1.5\%$ $(L=12)$ and 0.47% $(L=16)$ from (4.3) for $m_q=0.01$ while the data in Fig. 15 give 31% $(L=12)$ and 13% $(L=16)$.

Let us remark that the positive sign as well as the smallness of the size effect for the nucleon predicted by (4.3) is not an obvious result. In fact the positive contribution to the three-point coupling term is almost compensated by the integral of the pole contribution in $F_{\pi N}$. The integral of the nonpole part comes out positive because the integrand $\bar{F}_{\pi N}$ is negative for small values of p which dominate the integral. The smallness of the magnitude of the size effect originates from the cancellation above and also from the presence of powers of m_π/m_N, while the corresponding factor m_π/f_π leads to an enhancement for the pion case.

We have seen that the mass shift predicted by (4.1) is obviously far too small to account for the size dependence observed in Fig. 15. In fact the size dependence is well described by a power law of the form

$$m_H(L)=m_H(\infty)+\frac{c}{L^\alpha} \tag{4.6}$$

with $\alpha=2$–3 rather than an exponential [40]. This is illustrated in Fig. 17 where we plot the masses of π, ρ, and N as a function of $1/L^3$ together with the fit (4.6) with $\alpha=3$. The fit is excellent, especially for ρ and N. We should remark that other types of power behaviors such as $m_H(L)^2=m_H(\infty)^2+c/L^\alpha$ $(\alpha=2$–$3)$ also fit data. This indicates that the conspicuous size dependence is not due to propagation of pions around the lattice as summarized in the formula (4.1), but rather arises from the size of hadrons squeezed on the finite lattice used for simulations. The fact that the size effect is larger for the nucleon than for π and ρ also supports this view.

We may understand the power behavior in the following simple argument. Let us suppose that quarks are bound by some confining potential and let r_0 be the length scale characterizing the decrease of the wave function $\psi(r)$ for large r. One may mimic the squeezing of the wave function due to a finite lattice size by a replacement $r_0\to r_0'\propto L$. A sharper variation of the squeezed wave function leads to an increase of the kinetic energy of the ground state as L^{-2}. The detail of the index of power depends upon an adopted model and assumptions, but the

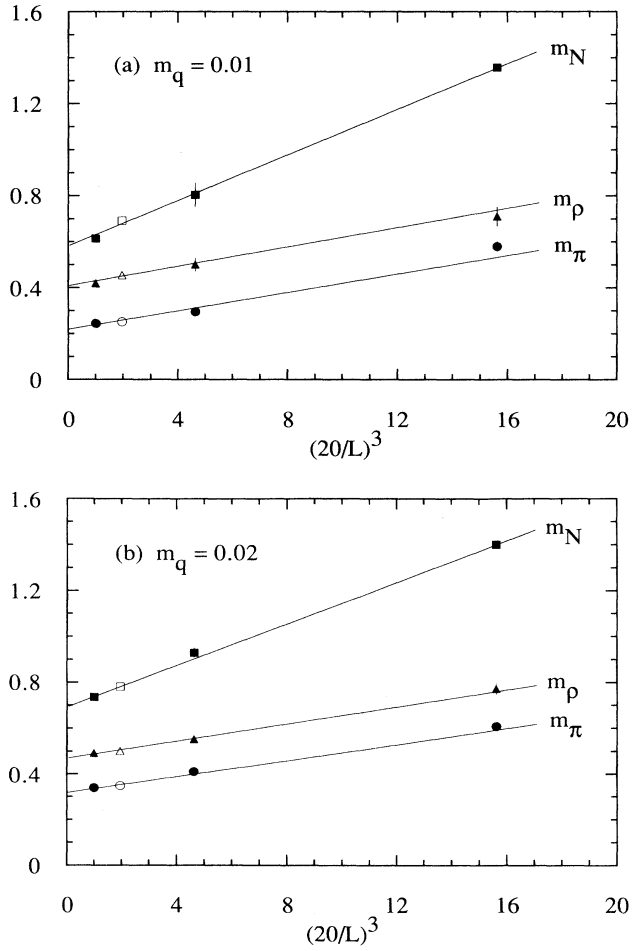

FIG. 17. Masses of $\pi(\gamma_5\xi_5)$, $\rho(\gamma_k\xi_k)$ and local nucleon (N) plotted as a function of $1/L^3$ and their linear fits (solid lines). Open symbols are the data of the Columbia group for $L=16$. (a) $m_q=0.01$, (b) $m_q=0.02$.

power behavior is generally expected from such a simple nonrelativistic quark model picture.

We should remark that the argument above assumes a Dirichlet-type boundary condition in which the wave function at the boundary is kept small. In lattice QCD this would happen if the amplitude of a quark propagating around the lattice cancels that in which the quark does not go through the boundary, and this appears to correspond to the periodic boundary condition for quark fields. On the other hand, if one changes the quark boundary condition to antiperiodic, the two types of amplitudes would contribute additively. The wave function becomes smoother in this case, leading to a decrease of meson masses [41]. (This situation resembles the case for the nonrelativistic quark model solved with the periodic boundary condition in a finite box.) To check this point we recalculated the meson spectrum for the $L=8$ lattice at $m_q=0.01$ with the antiperiodic boundary condition. We then found that the pion mass takes a value 0.221(6) and the ρ mass a value 0.248(37), both of which drastically differ from the values $m_\pi=0.581(22)$ and $m_\rho=0.711(42)$ obtained with the periodic boundary condition, and are also substantially smaller than the corresponding masses on an $L=20$ lattice; $m_\pi=0.2451(23)$ and $m_\rho=0.4184(70)$.

One should note that there is another important source of size effects for small lattice sizes, arising from the fact that the U(1) chiral symmetry of the Kogut-Susskind fermion action cannot be spontaneously broken for small spatial volumes. A rough estimate of the size L_c at which this type of size effect becomes important may be made by regarding one of the spatial axes as time and considering the system to be at an effective temperature $T_{\rm eff}=1/La$. From the fact that chiral symmetry becomes restored above a critical temperature T_c one expects a significant effect in hadron masses for lattice sizes smaller than $L_c\approx 1/T_c a$. Using the recent estimate $T_c\approx 150$ MeV for two light-quark flavors [42] and $a^{-1}=2.23$ GeV, we obtain $L_c\approx 15$. The absence of spontaneous breakdown of chiral symmetry leads us to expect a number of consequences. The mass of the pion will increase for a smaller L since it is no longer constrained to vanish at $m_q=0$ by the Nambu-Goldstone theorem. In the symmetric phase chiral symmetry should be satisfied by the degeneracy of π and σ, ρ and a_1, and of nucleon N and its negative parity partner N^-. In Fig. 15 we observe an increase of the pion mass. In addition Fig. 18 indeed shows the expected degeneracy between parity partners as chiral symmetry restores for a small L, similar to the behavior observed in the high-temperature phase of QCD [43].

We may conclude that, while an overall decrease of hadron mass with an increasing L is to be ascribed to a hadron size effect, lifting of the degeneracy is accounted for by a gradual spontaneous breakdown of chiral symmetry as L increases.

C. Hadron mass ratio

We plot in Fig. 19 the mass ratios m_N/m_ρ vs $(m_\pi/m_\rho)^2$ at $\beta=5.7$ using the data for the spatial size $L=20$ and $m_q=0.01$ and 0.02 (solid circles; see Table IX for numerical values). The data of the Columbia group [4] for $L=16$ (open circles) are taken for $m_q=0.01$, 0.015, 0.02, and 0.025 from left to right in the figure. The curves for an empirical quark-model mass formula [44] and that of the chiral perturbation theory are also shown.

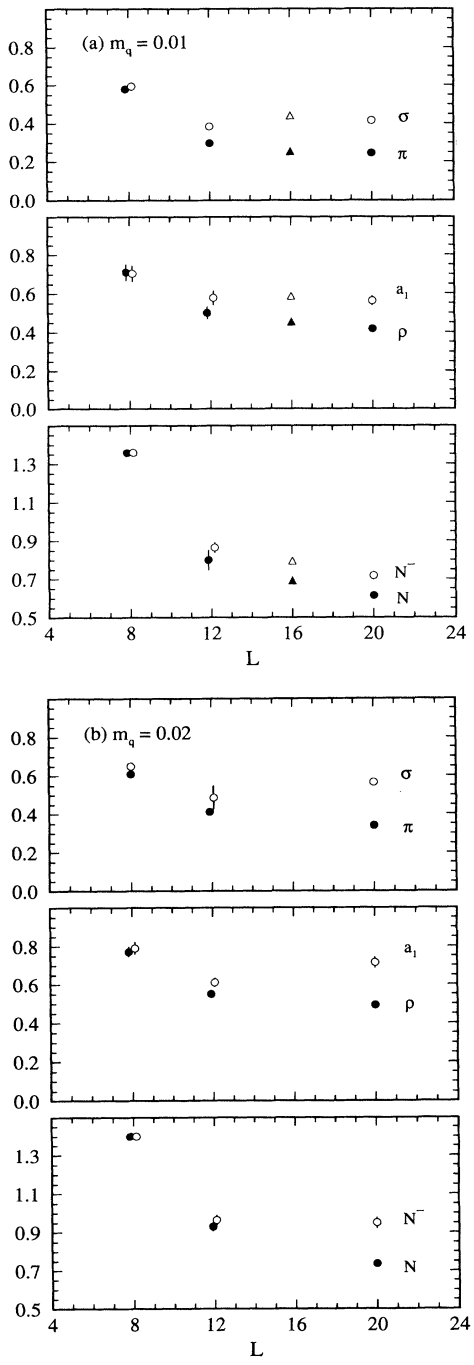

FIG. 18. Spatial size dependence of masses of parity partners $\pi(\gamma_5\xi_5)-\sigma(1)$, $\rho(\gamma_k\xi_k)-a_1(\gamma_k\gamma_5\xi_k\xi_5)$, and $N-N^-$ [B(I) operator] for (a) $m_q=0.01$ and (b) $m_q=0.02$. Triangles are data of Ref. [4].

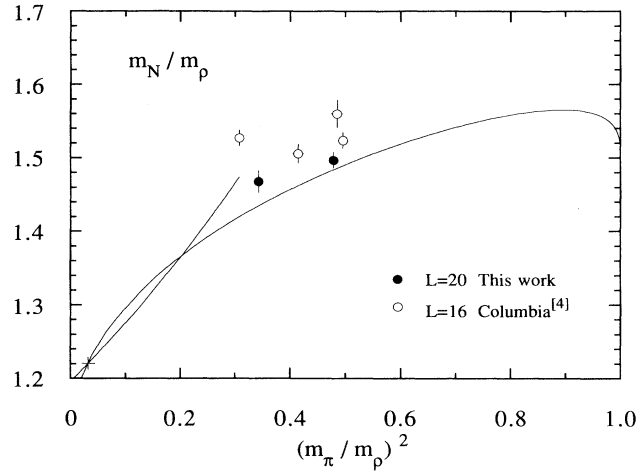

FIG. 19. Comparison of $L=16$ [4] (open symbols) and $L=20$ (solid symbols) data for the mass ratios m_N/m_ρ vs $(m_\pi/m_\rho)^2$ at $\beta=5.7$ for two flavors of dynamical KS fermions. Data for the operators $\pi(\gamma_5\xi_5)$, $\rho(\gamma_k\xi_k)$ and local nucleon are used. Solid lines represent the behavior expected from chiral perturbation theory and a quark model [44].

At $m_q=0.01$ a downward shift of m_N/m_ρ is seen as the lattice size is increased from $L=16$ to $L=20$. This is due to a larger finite size shift for the nucleon mass than for the ρ meson mass. Consequently the value of m_N/m_ρ for $L=20$ is closer to the prediction of the empirical quark-model mass formula than for $L=16$. A downward shift of m_N/m_ρ is also observed for $m_q=0.02$. For this case, however, an irregular behavior of the Columbia data for $m_q=0.025$–0.015 has to be resolved to conclude that the discrepancy is a real finite-size effect.

We attempt to estimate the value of the ratio m_N/m_ρ in the infinite volume limit from the available data. If we use the linear extrapolation (4.6) of m_N and m_ρ in $1/L^3$ we obtain $m_N/m_\rho=1.424(40)$ at $L=\infty$ for $m_q=0.01$ as compared to the value $m_N/m_\rho=1.468(15)$ for $L=20$. Alternatively one may extrapolate m_N/m_ρ linearly in $1/L^3$, which gives $m_N/m_\rho=1.452(17)$ at $L=\infty$. If we use the form $m_N/m_\rho=r_0+r_1/L^2$, we would find $m_N/m_\rho=1.386(14)$ instead. While there is a significant ambiguity in these extrapolations these analyses clearly indicate that the value of m_N/m_ρ measured on a lattice with a spatial size of the order of 2 fm suffers from substantial finite-size effects for full QCD.

Let us compare our results at $\beta=5.7$ for $m_q=0.01$ and 0.02 with those of the HEMCGC Collaboration at $\beta=5.6$ with $m_q=0.01$ and 0.025 [3]. At the quark mass of $m_q=0.01$ the HEMCGC Collaboration reported results for $L=12$ and $L=16$ lattice sizes. As is seen in Fig. 20 their ratio m_N/m_ρ decreases over these lattice sizes, exhibiting a finite-size effect similar in magnitude to what we found for $\beta=5.7$ between $L=16$ to 20. In addition their data are relatively higher and shifted left compared to our data. The leftward shift can be naturally understood; with $m_q=0.01$ fixed in lattice units the quark mass in physical units increases with β and therefore the ratio m_π/m_ρ should also increase. In order to understand the downward shift we recall that the lattice spacing at $\beta=5.7$ estimated from the ρ meson mass is equal to $a=(2.23\ \mathrm{GeV})^{-1}=0.089$ fm. A similar estimation at $\beta=5.6$ for the data of HEMCGC Collaboration gives $a=(1.81\ \mathrm{GeV})^{-1}=0.11$ fm. The physical lattice size used at the two values of β is comparable; $La=1.77$ fm for HEMCGC on a 16^3 lattice at $\beta=5.6$ and 1.78 fm for our data on a 20^3 lattice at $\beta=5.7$. Therefore we expect the magnitude of finite-size effects to be similar for the two simulations. We then conclude that the decrease of m_N/m_ρ should be attributed to the finite-lattice-spacing effect. In quenched hadron mass calculations a decrease of m_N/m_ρ with an increasing β has previously been seen [45].

V. CHIRAL SYMMETRY

A. Chiral order parameter

The Kogut-Susskind fermion formulation retains a U(1) subgroup of chiral symmetry. The order parameter of this symmetry is the chiral condensate $\langle\bar{\chi}\chi\rangle$. In Table IV we have listed the values of $\langle\bar{\chi}\chi\rangle$ measured at $\beta=5.7$ on an L^4 lattice for $L=8$–20 as a function of the quark mass m_q. The values at $m_q=0$ obtained by a linear extrapolation $\langle\bar{\chi}\chi\rangle=Am_q+B$ are plotted in Fig. 21 (see Table VII for numerical values of A and B). A nonzero value of $\langle\bar{\chi}\chi\rangle$ at $m_q=0$ for large L (e.g., $L=20$) shows that chiral symmetry is spontaneously broken. We also observe that the magnitude of $\langle\bar{\chi}\chi\rangle$ decreases for a smaller L and drops rather abruptly between $L=12$ and $L=8$ with the $m_q=0$ extrapolation becoming consistent

TABLE IX. Mass ratios for full QCD with two dynamical flavors of KS fermions at $\beta=5.7$ obtained with $\pi(\gamma_5\xi_5)$, local nucleon N, and $\rho(\gamma_k\xi_k)$ or $\rho(\gamma_k\gamma_4\xi_k\xi_4)$. Errors are estimated by the jack-knife method with the bin size $\tau_{\mathrm{bin}}=50$.

	$20^3\times(20\times2)$		$16^3\times(16\times2)$		$12^3\times(12\times3)$		$8^3\times(16\times2)$	
m_q	0.01	0.02	0.01	0.02	0.01	0.02	0.01	0.02
$m_\pi/m_{\rho(\gamma_k\xi_k)}$	0.5858(64)	0.6923(50)	0.612(17)	0.685(14)	0.593(31)	0.746(22)	0.817(31)	0.789(29)
$m_N/m_{\rho(\gamma_k\xi_k)}$	1.468(15)	1.497(11)	1.558(97)	1.512(22)	1.609(92)	1.685(48)	1.91(11)	1.814(61)
$m_\pi/m_{\rho(\gamma_k\gamma_4\xi_k\xi_4)}$	0.590(12)	0.6819(50)	0.581(19)	0.6856(79)	0.609(19)	0.775(19)	0.860(60)	0.806(31)
$m_N/m_{\rho(\gamma_k\gamma_4\xi_k\xi_4)}$	1.479(26)	1.474(11)	1.478(77)	1.514(15)	1.65(12)	1.751(40)	2.01(19)	1.852(61)

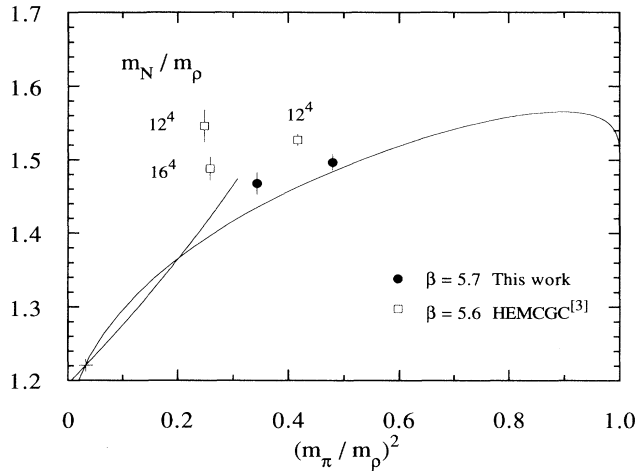

FIG. 20. Comparison of mass ratios for $\beta=5.6$ (open squares) and $\beta=5.7$ (solid circles). Meaning of solid lines are the same as in Fig. 19.

with zero for $L=8$. These results reflect the fact that a spontaneous breakdown of symmetry does not occur for small volumes.

There have been analytical studies of finite-size effects on the dynamics of a spontaneously broken phase in the context of scalar field theories and chiral Lagrangians [15–17]. In these theories Nambu-Goldstone bosons start propagating around the lattice as the lattice size decreases from infinity. This effect becomes significant for a size $L\sim 1/m_{\mathrm{NG}}$ with m_{NG} the Nambu-Goldstone boson mass. For a yet smaller size of order $L\sim/\sqrt{m_{\mathrm{NG}}}$ the zero mode of the order-parameter field starts to fluctuate largely, resulting in a decrease of its expectation value and the restoration of the symmetry. In our case of QCD with two flavors of Kogut-Susskind quarks the system has $\mathrm{U}(1)\equiv\mathrm{O}(2)$ chiral symmetry at a finite lattice spacing which is expected to be enhanced to $\mathrm{SU}(2)\otimes\mathrm{SU}(2)\equiv\mathrm{O}(4)$ symmetry in the continuum limit. For a comparison of

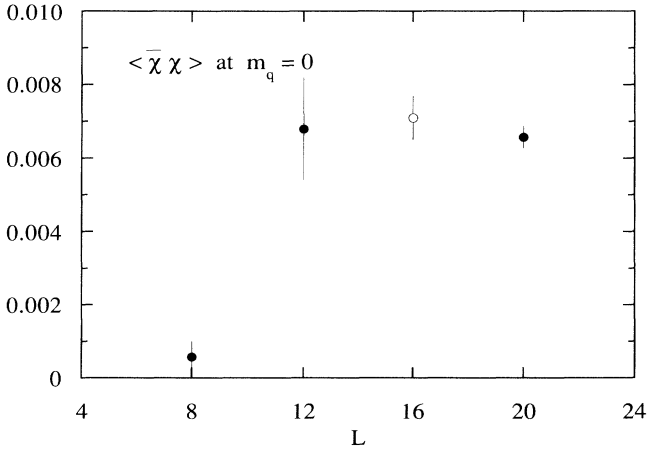

FIG. 21. Lattice size dependence of chiral order parameter at $\beta=5.7$ linearly extrapolated to $m_q=0$.

data with analytic predictions one may therefore use the results obtained for the $\mathrm{O}(n)$-invariant nonlinear σ model as an effective Lagrangian.

For the chiral order parameter $\Sigma=\langle\bar{\chi}\chi\rangle$ the analytic result for a box of a size L^4 is given by [15,17]

$$\frac{\Sigma(L)}{\Sigma(\infty)}=\rho\frac{Y_n'(\rho z^4(f_\pi/m_\pi)^2)}{Y_n(\rho z^4(f_\pi/m_\pi)^2)}\ , \tag{5.1}$$

where m_π and f_π are the infinite volume values of the pion mass and the pion decay constant, $z=m_\pi L$, $Y_n(x)=(x/2)^{-(n-2)/2}I_{(n-2)/2}(x)$ with $I_k(x)$ the modified Bessel function, and

$$\rho=1-\frac{n-1}{2}\frac{m_\pi^2}{f_\pi^2}\frac{1}{z^2}G(z) \tag{5.2}$$

with

$$G(z)=\frac{1}{16\pi^2}\int_0^\infty\frac{dt}{t^2}e^{-tz^2}\sum_{n\in\mathbb{Z}^4-\{0\}}e^{-n^2/4t}-\frac{1}{z^2}\ . \tag{5.3}$$

This formula smoothly interpolates the two regions $L\sim 1/m_\pi$ and $L\sim 1/\sqrt{m_\pi}$ discussed above. For L large with $L\sim 1/m_\pi$ a straightforward expansion of (5.1) in inverse powers of L gives

$$\frac{\Sigma(L)}{\Sigma(\infty)}=1-\frac{n-1}{2}\frac{m_\pi^2}{f_\pi^2}\left[\frac{2}{\pi^3}\right]^{1/2}\frac{1}{z^{3/2}}e^{-z}+O(e^{-\sqrt{2}z})\ . \tag{5.4}$$

The second term represents the one-pion loop finite-size correction similar to those given in (4.1). For $L\sim 1/\sqrt{m_\pi}$ the variable $z=m_\pi L=m_\pi L^2/L$ should be regarded as small. Replacing $G(z)$ by $G(0)=-\beta_1=-0.140\,461$ in (5.2) the right-hand side of (5.1) coincides with the formula given in Ref. [17].

In Fig. 22 the value of $\langle\bar{\chi}\chi\rangle$ at $\beta=5.7$ is plotted as a

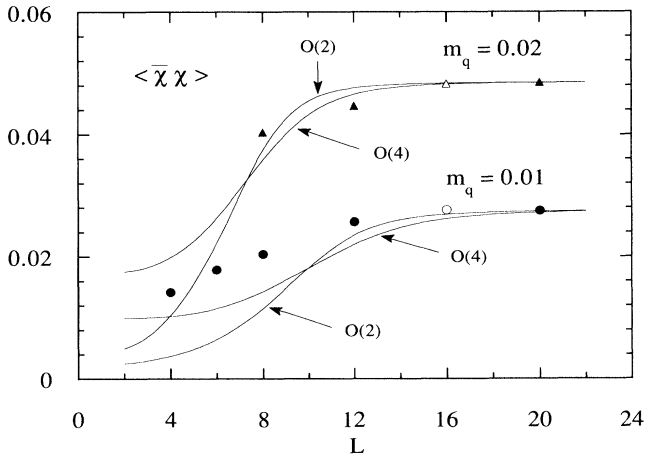

FIG. 22. Lattice size dependence of chiral order parameter for $\beta=5.7$ at $m_q=0.01$ (circles) and $m_q=0.02$ (triangles). Open symbols are data of Ref. [4]. Solid lines are prediction of chiral perturbation theory [see (5.1) of text] for O(2) and O(4) symmetries.

function of L for $m_q=0.01$ and 0.02. The solid curves are obtained from (5.1) where we substituted the values measured on a 20^4 lattice for $\Sigma(\infty)$ and m_π and used $f_\pi=0.0421$ of (5.13) below. The curves for O(2) as well as for O(4) symmetry are drawn since identification of the symmetry group is ambiguous at a finite lattice spacing. We observe that neither of these curves lend good fit to data, especially for the lattice size below $L\approx 10-12$.

There are several possible reasons for the discrepancy. A basic assumption for the validity of the use of the effective chiral Lagrangian is that states other than the pion have masses much larger than m_π. This is not quite satisfied in our case (e.g., $m_\rho/m_\pi=1.71$ for $m_q=0.01$). Second, the description in terms of chiral Lagrangians may not be applicable for lattice sizes so small that the system is effectively in the high-temperature phase. To illustrate this point we note that the value of the chiral order parameter $\langle\bar{\chi}\chi\rangle$ becomes small for each gauge configuration for such lattice sizes, while in the chiral Lagrangian approach the smallness of $\langle\bar{\chi}\chi\rangle$ is a consequence of large fluctuations of the order parameter.

B. PCAC relation for the pion mass

The argument based on current algebra and PCAC predicts that the Nambu-Goldstone pion mass should behave as

$$m_\pi^2 \propto m_q \tag{5.5}$$

for small quark masses. Whether simulation data satisfy this relation provides an important check on the spontaneous breakdown of chiral symmetry. In the Kogut-Susskind fermion formalism there are 15 flavor nonsinglet pseudoscalar particles. Only one of them is associated with the U(1) chiral symmetry and hence is expected to satisfy (5.5) at a finite lattice spacing. The remaining 14 particles may generally have a nonvanishing mass at $m_q=0$. They, however, should tend to zero toward the continuum limit where a restoration of full flavor symmetry is expected.

Our wall source enables us to measure the masses of three pions $\pi(\gamma_5\xi_5)$, $\pi(\gamma_4\gamma_5\xi_4\xi_5)$ and $\pi(\gamma_5\xi_3\xi_5)$ of which $\pi(\gamma_5\xi_5)$ is the Nambu-Goldstone pion corresponding to U(1) chiral symmetry. Figure 23 shows the lattice size dependence of the Nambu-Goldstone pion mass squared at $m_q=0$ estimated by a linear extrapolation $m^2_{\pi(\gamma_5\xi_5)}=A_\pi m_q+B_\pi$ (see Table VII for numerical values of A_π and B_π). We observe that quite a large value of B_π for $L=8$ drops abruptly between $L=8$ and 12. This behavior is consistent with that of $\langle\bar{\chi}\chi\rangle_{m_q=0}$ shown in Fig. 21 in that they both indicate that the restoration of U(1) chiral symmetry occurs at $L\sim 10$ in a fairly abrupt manner. We add in this connection that a recent finite-temperature simulation with eight time slices [46] found a crossover from the low to the high temperature phase at $\beta\approx 5.5-5.6$. This is below the value $\beta=5.7$ for our simulation, and hence consistent with these findings. The exact correspondence between the finite-temperature transition and the restoration of chiral symmetry for small spatial volumes is a little obscure, however, since the geometry of the lattice and the boundary condition for quark fields (we use the periodic boundary condition in all four directions) are different.

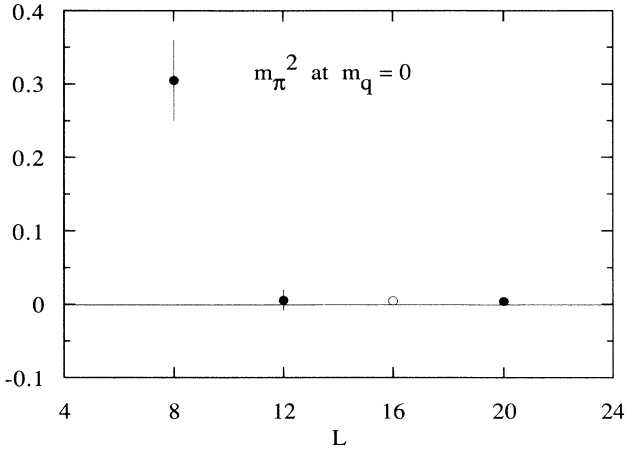

FIG. 23. Nambu-Goldstone pion mass squared at $m_q=0$ as a function of the spatial lattice size L. The open symbol at $L=16$ is obtained from the data of Ref. [4] at $m_q=0.01$ and 0.02.

It should be noted that the intercept B_π does not quite vanish for $L\geq 12$, which may be ascribed to finite-size effects. The rate of decrease of B_π from $L=12$ to $L=20$ seems slow compared to the behavior $m_\pi\sim 1/f_\pi L^3$ at $m_q=0$ expected from chiral Lagrangians [16]. For $L=20$ we have

$$m^2_{\pi(\gamma_5\xi_5)}=0.0043(25)+5.57(16)m_q\ . \tag{5.6}$$

In Fig. 24 we compare the masses of the three pions $\pi(\gamma_5\xi_5)$, $\pi(\gamma_4\gamma_5\xi_4\xi_5)$, and $\pi(\gamma_5\xi_3\xi_5)$ obtained on an $L=20$ lattice. The fits for the last two pions are given by

$$\begin{aligned} m^2_{\pi(\gamma_4\gamma_5\xi_4\xi_5)}&=0.0090(67)+6.99(38)m_q\ , \\ m^2_{\pi(\gamma_5\xi_3\xi_5)}&=0.0151(39)+6.55(24)m_q\ . \end{aligned} \tag{5.7}$$

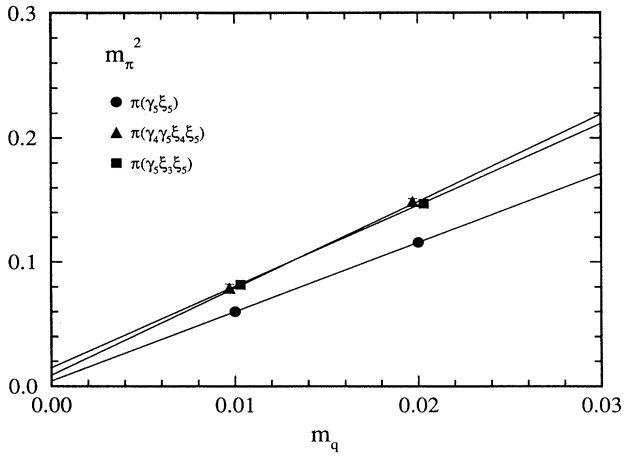

FIG. 24. Quark mass dependence of $m^2_{\pi(\gamma_5\xi_5)}$, $m^2_{\pi(\gamma_4\gamma_5\xi_4\xi_5)}$, and $m^2_{\pi(\gamma_5\xi_3\xi_5)}$ on a $20^3\times(20\times 2)$ lattice at $\beta=5.7$.

The masses of $\pi(\gamma_4\gamma_5\xi_4\xi_5)$ and $\pi(\gamma_5\xi_3\xi_5)$ are about 15% higher than that of the Nambu-Goldstone pion at $m_q=0.01$ and 0.02 reflecting the breaking of flavor symmetry. They, however, extrapolate to fairly small values at $m_q=0$ supporting that they would become massless in the limit of continuous space-time.

C. Pion decay constant [47]

The definition of the pion decay constant in the continuum is given by

$$\sqrt{2}f_\pi m_\pi=\langle 0|\bar{u}\gamma_4\gamma_5 d|\pi^+(\mathbf{p}=0)\rangle \ . \tag{5.8}$$

Using PCAC this equation may be rewritten as

$$\sqrt{2}f_\pi m_\pi^2=(m_u+m_d)\langle 0|\bar{u}\gamma_5 d|\pi^+(\mathbf{p}=0)\rangle \tag{5.9}$$

and an application of current algebra leads to

$$f_\pi^2 m_\pi^2=(m_u+m_d)\langle \tfrac{1}{2}(\bar{u}u+\bar{d}d)\rangle \ . \tag{5.10}$$

These relations provide three ways of estimating the pion decay constant.

A lattice transcription of the condensate $\langle \bar{u}u\rangle$ is given by $\frac{3}{4}\langle\bar{\chi}\chi\rangle$ since a Kogut-Susskind fermion field gives rise to four continuum flavors (the factor 3 is due to our normalization of $\langle\bar{\chi}\chi\rangle$). For the case of two degenerate flavors $m_u=m_d=m_q$ the relation (5.10) becomes

$$f_\pi=\left[\frac{3m_q\langle\bar{\chi}\chi\rangle_{m_q=0}}{2m_\pi^2}\right]^{1/2} \ . \tag{5.11}$$

We note that this method yields f_π only at zero quark mass; for $m_q\neq 0$ quadratically divergent short-distance contributions have to be removed from $\langle\bar{\chi}\chi\rangle$ to all orders of perturbation theory [25].

We evaluate the left hand side of (5.11) using (5.6) and

$$\langle\bar{\chi}\chi\rangle=0.006\,58(30)+2.097(19)m_q \tag{5.12}$$

obtained on a 20^4 lattice, and find

$$f_\pi=0.0421(11)(16) \ , \tag{5.13}$$

where the second error accounts for systematic errors arising from the nonvanishing of m_π at $m_q=0$. With $a^{-1}=2.23(9)$ GeV this value translates into 94(5)(4) MeV in physical units, which is in a good agreement with the experimental value 93 MeV.

Let us now turn to an extraction of f_π from (5.8) and (5.9). For Kogut-Susskind fermions these relations may be replaced by

$$\begin{aligned}&\sqrt{2}f_\pi m_\pi=\langle 0|A_4|\pi\rangle \ ,\\ &\sqrt{2}f_\pi m_\pi^2=2m_q\langle 0|P|\pi\rangle \ ,\end{aligned} \tag{5.14}$$

with the lattice axial-vector current A_μ and the pseudoscalar density P defined by

$$\begin{aligned}&A_\mu(n)=\tfrac{1}{2}\epsilon(n)\eta_\mu(n)[\bar{\chi}(n+\hat{\mu})U_\mu(n)^\dagger\chi(n)-\text{H.c.}] \ ,\\ &P(n)=\epsilon(n)\bar{\chi}(n)\chi(n) \ .\end{aligned} \tag{5.15}$$

The link variable U_μ is inserted to make the operator A_μ gauge invariant. Since we fix link variables to a gauge we also used the operator without the factor U_μ,

$$A'_\mu(n)=\tfrac{1}{2}\epsilon(n)\eta_\mu(n)[\bar{\chi}(n+\hat{\mu})\chi(n)-\text{H.c.}] \ . \tag{5.16}$$

For the gauge invariant current A_μ the PCAC relation

$$\nabla_\mu A_\mu(n)=2m_q P(n) \tag{5.17}$$

holds due to U(1) chiral symmetry of the Kogut-Susskind fermion action. The two equations in (5.14) therefore should yield identical values for f_π, which provides a check on the reliability of numerical results. On the other hand, the gauge noninvariant current A'_μ requires a finite renormalization as we shall discuss below.

The matrix elements appearing in (5.14) are extracted from the large-time behavior of the correlation functions at zero spatial momentum:

$$\begin{aligned}C_{WA}(t)&=\langle W(0)A(t)\rangle\\ &\to\frac{\langle 0|W|\pi\rangle\langle\pi|A|0\rangle}{2m_\pi V_s}e^{-m_\pi(t+1/2)} \ ,\\ C_{WP}(t)&=\langle W(0)P(t)\rangle\\ &\to\frac{\langle 0|W|\pi\rangle\langle\pi|P|0\rangle}{2m_\pi V_s}e^{-m_\pi t} \ ,\\ C_{WW}(t)&=\langle W(0)W(t)\rangle\\ &\to\frac{\langle 0|W|\pi\rangle\langle\pi|W|0\rangle}{2m_\pi V_s}e^{-m_\pi t} \ ,\end{aligned} \tag{5.18}$$

where V_s is the spatial lattice volume, $A=A_4$ or A'_4 and $W(t)$ is a wall source for the Nambu-Goldstone pion. The factor $e^{-1/2m_\pi}$ in C_{WA} takes into account the fact that the operator A is extended over a timelike link and hence it is natural to measure the temporal separation from its midpoint.

For the wall source we use the operator

$$W(t)=\sum_{\mathbf{n}}\sum_{\mathbf{n}'}[\epsilon(\mathbf{n})+\epsilon(\mathbf{n}')]\bar{\chi}(\mathbf{n},t)\chi(\mathbf{n}',t) \ . \tag{5.19}$$

This wall creates only the Nambu-Goldstone pion among 15 pions. (It couples to various ρ mesons, however, which contaminate signals for small t.) A practical complication in the use of (5.18) is that the hybrid gauge we used for the spectrum calculation is not suitable for an extraction of $\langle 0|W|\pi\rangle$. This is because the coupling of the wall to the pion at time $t\neq 0$ where links are fixed to the Landau gauge is different from that at time $t=0$ with the Coulomb gauge fixing. We have therefore recalculated the correlation functions (5.18) using the Coulomb and the Landau gauge fixings for the entire lattice. For this calculation we used 26 configurations separated by 25 time units for a $20^3\times(20\times 2)$ lattice at $\beta=5.7$ and $m_q=0.01$ and 20 configurations for $m_q=0.02$ with the same time separation.

For C_{WA} and C_{WP} we observed a plateau in the effective mass for $t\gtrsim 10$ and the residues are estimated by a single hyperbolic cosine fit for $30\geq t\geq 10$. The statistical quality of signals is poorer for C_{WW}. We estimate the matrix element $\langle 0|W|\pi\rangle$ by fitting C_{WW} over $22\geq t\geq 18$

using m_π determined from C_{WP} as input. Typical propagators and effective masses are shown in Figs. 25 and 26. The results for the pion mass and the pion decay constant are summarized in Table X. We note that the values of the pion mass extracted from C_{WA} and C_{WP} are consistent with those obtained from the full set of configurations (see Table V).

Lattice results for the decay constant generally have to be corrected by a wave function renormalization factor Z relating the lattice and continuum operators $\mathcal{O}^{\text{continuum}}=Z\mathcal{O}^{\text{lattice}}$. An exception is the gauge invariant axial-vector current A_μ which corresponds to the axial U(1) symmetry of the Kogut-Susskind fermion formalism and hence $Z=1$. For the gauge-noninvariant current A'_μ a one-loop calculation [48,49] in the Landau gauge [49] gives

$$Z^{A'}=1-\frac{1}{2}g^2 z_{0000}+O(g^4) \tag{5.20}$$

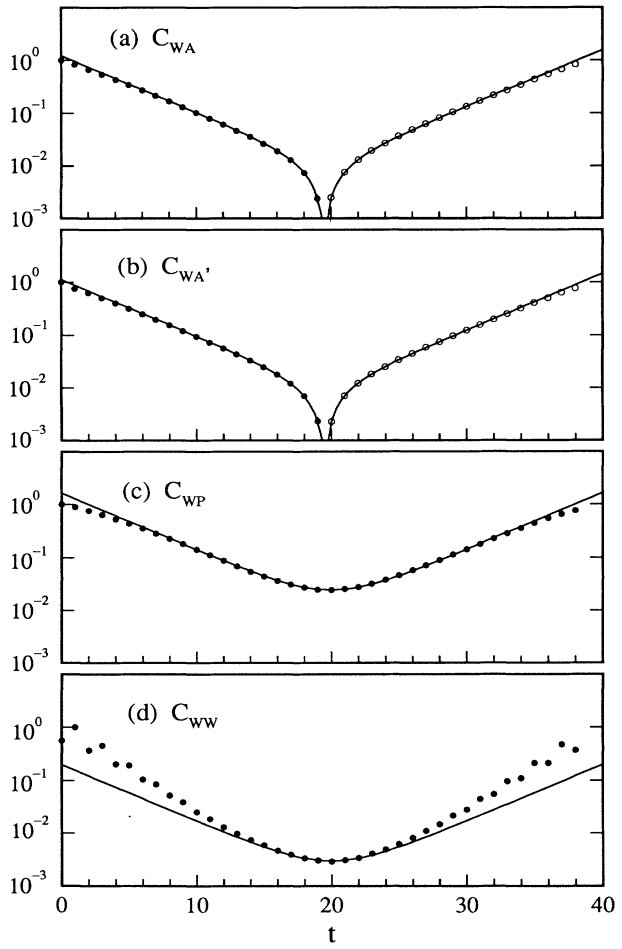

FIG. 25. Propagators (a) $C_{WA_4}(t)$, (b) $C_{WA'_4}(t)$, (c) $C_{WP}(t)$, and (d) $C_{WW}(t)$ in the Landau gauge for $m_q=0.01$ normalized to unity at $t=0$ ($t=1$ for C_{WW}). Open circles mean negative values. Solid lines are fits over $30\geq t\geq 10$ for (a)–(c) and $22\geq t\geq 18$ for (d) [with m_π taken from the fit of (c)] as described in text.

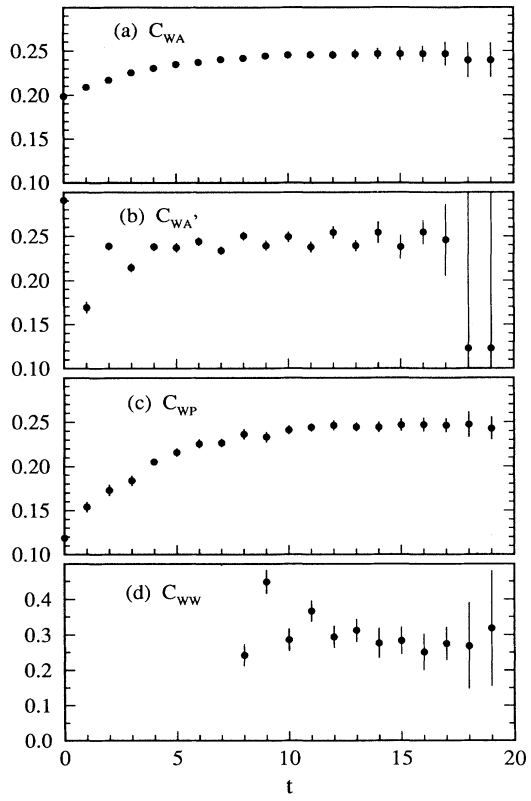

FIG. 26. Effective masses for the propagators of Fig. 25.

with $z_{0000}=0.154\,933\,39\ldots$. Numerically the correction factor for A'_μ is -8.2% at $\beta=5.7$. The one-loop corrected values of the decay constant are also listed in Table X. The Z factor for the pseudoscalar density P is logarithmically divergent. The divergence, however, is canceled by that of the quark mass. Explicit calculations [48,49] show that finite renormalizations also cancel for Kogut-Susskind fermions up to possible corrections of order $m_q a$. Thus f_π extracted from the pseudoscalar density does not require renormalizations to this accuracy.

We see in Table X that the values of f_π obtained from the pseudoscalar density P agrees with those from the gauge invariant current A_4 within each type of gauge fixing as is expected from (5.17). There is a trend that the Landau gauge results for the operators P and A_4 are smaller than those for the Coulomb gauge. We consider that this is due to low statistics, especially in the C_{WW} propagator, the signal of which is rather poor. We also note that the uncorrected values for the gauge noninvariant current A'_4 in the Landau gauge are systematically larger than those from the gauge invariant current A_4. It is interesting to observe that the one-loop correction (5.20) reduces these values significantly, making the corrected values quite consistent with the other estimates in the Landau gauge.

The quark mass dependence of the decay constant, one-loop corrected by (5.20) for the gauge noninvariant current A'_4, is plotted in Fig. 27 where the leftmost point is the estimate (5.13) based on (5.11). The value of f_π

TABLE X. Pion decay constant f_π and pion mass m_π in lattice units extracted from correlation functions of several operators in Landau and Coulomb gauges with two flavors of KS fermions at $\beta=5.7$ for $m_q=0.01$ and 0.02. For the gauge-noninvariant operator A' in the Landau gauge one-loop-corrected values are also listed.

		$m_q=0.01$		$m_q=0.02$	
Operator	Gauge	m_π	f_π	m_π	f_π
A	Landau	0.2465 ±0.0050	0.0498 ±0.0016	0.3417 ±0.0024	0.0554 ±0.0017
	Coulomb	0.2498 ±0.0028	0.0542 ±0.0017	0.3443 ±0.0027	0.0611 ±0.0017
A'	Landau	0.2467 ±0.0052	0.0572 ±0.0019	0.3421 ±0.0023	0.0628 ±0.0020
	Landau (corr.)		0.0525 ±0.0017		0.0577 ±0.0018
P	Landau	0.2451 ±0.0037	0.0490 ±0.0011	0.3431 ±0.0028	0.0565 ±0.0022
	Coulomb	0.2461 ±0.0031	0.0521 ±0.0009	0.3438 ±0.0029	0.0609 ±0.0018

linearly extrapolated to $m_q=0$ is given in Table XI. We find that f_π at $m_q=0$ from the correlation functions takes values in the range 93(8)–105(9) MeV, which is consistent with the value 94(5)(4) MeV obtained with (5.11) within 10%.

D. Mass splitting between parity partners

The mass splitting of the nucleon N and its negative parity partner N^- arises from spontaneous breakdown of chiral symmetry. Therefore one expects the mass splitting to become smaller for a smaller lattice size. As shown in Fig. 18 this behavior is clearly seen in our data, with the splitting becoming apparent only for $L \geq 16$. A similar behavior is also observed for the masses of parity partners π and σ, and ρ and a_1 (see Fig. 18). We also note that the almost complete degeneracy of the masses of parity partners for $L=8$ seen in Fig. 18 is consistent with the behavior of the chiral order parameter $\langle \bar{\chi}\chi \rangle$ and the pion mass m_π at $m_q=0$ (see Figs. 21 and 23) which show a complete restoration of chiral symmetry at this lattice size. These results are reminiscent of the restoration of chiral symmetry and the degeneracy of parity partners in the high-temperature phase of QCD first discussed in Ref. [43].

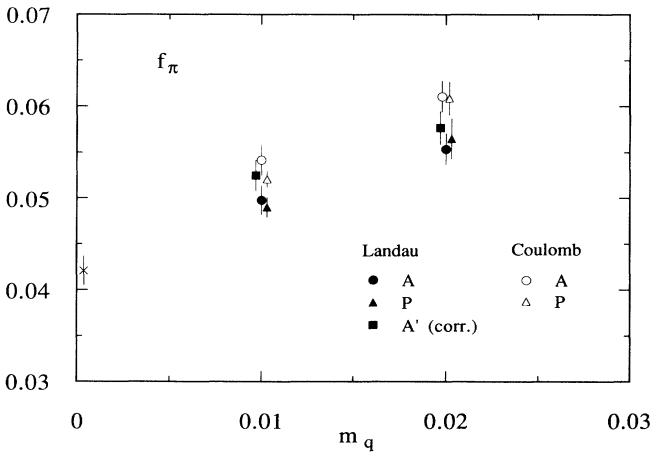

FIG. 27. Pion decay constant in lattice units as a function of m_q for full QCD with two flavors of KS quarks at $\beta=5.7$. For the gauge noninvariant current A_4' one-loop-corrected values are plotted. The left-most cross is the estimate at $m_q=0$ based on (5.11) of text.

TABLE XI. Pion decay constant f_π at $m_q=0$ obtained by a linear extrapolation of data in Table X. Values in the first column are in lattice units and those in the second column in physical units using $a^{-1}=2.23(9)$ GeV. The last row gives the value obtained with Eq. (5.11) of the text.

Operator	Gauge	f_π (lattice units)	f_π (MeV)
A	Landau	0.0442 ±0.0036	99 ±9
	Coulomb	0.0473 ±0.0038	105 ±9
A'	Landau (corr.)	0.0473 ±0.0038	105 ±9
P	Landau	0.0415 ±0.0031	93 ±8
	Coulomb	0.0433 ±0.0025	97 ±7
$\langle \bar{\chi}\chi \rangle$		0.0421 ±0.0011±0.0016	94 ±5±4

VI. CONCLUSION

In this work we have carried out an extensive analysis for the hadron mass spectrum at $\beta=5.7$ for two-flavor full QCD with the Kogut-Susskind fermion action. Our main emphasis is given to demonstrate that the full QCD hadron mass spectrum suffers from a significant lattice-size dependence even when the physical size of the lattice is of the order of 2 fm, for which size clear lattice-size dependence has not been reported from quenched spectroscopy. We have shown that the finite-lattice-size corrections for hadron masses are described well by a power law $L^{-\alpha}$ with $\alpha=2$–3, rather than an exponential e^{-mL} as predicted by analytic work for the virtual pion emission. We have suggested that the effect arises from an artificial squeezing of the spatial extent of hadrons. We have also shown that both the finite-size and the finite-lattice-spacing corrections bring the nucleon to ρ mass ratio in a better agreement with the experiment. This shows that finite-lattice-size effect must be taken into account, should one attempt to extract the hadron masses within an error of 2–3 %.

We have also studied the operator dependence of the hadron mass spectrum using the formalism of Golterman and Smit [19,20]. We have found that the result is basically operator-independent for the meson masses. For the nucleon, however, the mass depends on operators used up to 4%. In addition several nucleon operators yielded unexpectedly large masses which are close to the masses obtained from the operators which are assigned to the Δ baryon. Such operator-dependent results would be an origin of systematic errors for lattice hadron spectroscopy, and more extensive study for this aspect is desirable [27].

The chiral aspect of the full QCD hadron spectroscopy is also explored in some detail. It was found that the quark mass dependence of the pion mass is consistent with the relation predicted by PCAC $m_\pi^2 \propto m_q$. We have also shown that the pion decay constant is consistently determined within an accuracy of 10% with the aid of PCAC and from various correlators including the axial-vector current and the pseudoscalar density. The mass degeneracy between chiral partners is also lifted for a large spatial extent of the lattice, as anticipated. On the other hand, the quark mass extracted from the simulation does not agree with what we expect from the empirical studies using current algebra. Further exploration is needed in this respect to establish full consistency with the phenomenological theory of current algebra and PCAC.

For the simulation presented in this article we used about 5000 hours of CPU time on HITAC S820/80 at KEK with a sustained computing speed estimated to be 1.2 GFlops for our code for the hybrid R algorithm. About 75% of the CPU time is used to generate configurations for $m_q=0.01$ and 0.02 on a 20^4 lattice for our final spectroscopic result reported here.

ACKNOWLEDGMENTS

We would like to thank KEK for a very generous allowance of computer time and strong and extensive support throughout the two years that it took us to bring the present work to completion. We would also like to thank Georgio Parisi for a very important discussion on the power dependence of the size effect for hadron masses. This work was supported in part by the Grant-in-Aid of the Ministry of Education (No. 03640270, No. 4-7502).

[1] For an early attempt, see M. Fukugita, Y. Oyanagi, and A. Ukawa, Phys. Rev. Lett. **57**, 953 (1986); Phys. Rev. D **36**, 824 (1987); Phys. Lett. B **203**, 145 (1988). See also M. Campostrini, K. J. M. Moriarty, J. Potvin, and C. Rebbi, Phys. Lett. B **193**, 78 (1987); H. Hamber, *ibid.* **193** 292 (1987).

[2] S. Gottlieb, W. Liu, D. Toussaint, R. L. Renken, and R. L. Sugar, Phys. Rev. D **38**, 2245 (1988).

[3] HEMCGC Collaboration, K. M. Bitar *et al.*, Phys. Rev. D **42**, 3794 (1990). See also U. M. Heller, in *Lattice '91*, Proceedings of the International Symposium, Tsukuba, Japan, 1991, edited by M. Fukugita, Y. Iwasaki, M. Okawa, and A. Ukawa [Nucl. Phys. B (Proc. Suppl.) **26**, 259 (1992)].

[4] F. R. Brown, F. P. Butler, H. Cheng, N. H. Christ, Z. Dong, W. Schaffer, L. I. Unger, and A. Vaccarino, Phys. Rev. Lett. **67**, 1062 (1991); H. Chen, in *Lattice '90*, Proceedings of the International Symposium, Tallahassee, Florida, 1990, edited by U. M. Heller, A. D. Kennedy, and S. Sanielevici [Nucl. Phys. B (Proc. Suppl.) **20**, 370 (1991)].

[5] MT_c Collaboration, R. Altmeyer, K. D. Born, M. Göckeler, R. Horsley, E. Laermann, and G. Schierholz, Report No. HLRZ 92-17, 1992 (unpublished).

[6] R. Gupta, C. F. Baillie, R. G. Brickner, G. W. Kilcup, A. Patel, and S. R. Sharpe, Phys. Rev. D **44**, 3272 (1992).

[7] For a recent review, see, D. Toussaint, in *Lattice '91* [3], p. 3.

[8] APE Collaboration, S. Cabasino *et al.*, Phys. Lett. B **258**, 195 (1991); **258**, 202 (1991).

[9] QCDPAX Collaboration, T. Yoshié, Y. Iwasaki, K. Kanaya, S. Sakai, T. Hoshino, T. Shirakawa, and Y. Oyanagi, in *Lattice '91* [3], p. 281; and (private communication); T. Yoshié, Y. Iwasaki and S. Sakai, in *Lattice '89*, Proceedings of the International Symposium, Capri, Italy, 1989, edited by R. Petronzio *et al.* [Nucl. Phys. B (Proc. Suppl.) **17**, 413 (1990)].

[10] R. Gupta, G. Guralnik, G. W. Kilcup, and S. R. Sharpe, Phys. Rev. D **43** 2003 (1991).

[11] F. Butler, H. Chen, J. Sexton, A. Vaccarino, and D. Weingarten, in *Lattice '91* [3], p. 287.

[12] M. Fukugita, H. Mino, M. Okawa, and A. Ukawa, in *Lattice '90* [4], p. 376.

[13] C. W. Bernard *et al.*, in *Lattice '91* [3], p. 262.

[14] M. Lüscher, in *Progress in Gauge Field Theory*, Proceedings of the Cargèse Summer Institute, Cargèse, France, 1983, edited by G. 't Hooft *et al.*, NATO Advanced Study Institutes, Series B: Physics Vol. 115 (Plenum, New York, 1984); Commun. Math. Phys. **104**, 177 (1986).

[15] J. Gässer and H. Leutwyler, Phys. Lett. B **184**, 83 (1987); **188**, 477 (1987).

[16] H. Leutwyler, Phys. Lett. B **189**, 197 (1987).

[17] P. Hasenfratz and H. Leutwyler, Nucl. Phys. **B343**, 241 (1990).

[18] S. Gottlieb, W. Liu, D. Toussaint, R. L. Renken, and R. L. Sugar, Phys. Rev. D **35**, 2531 (1987).

[19] M. L. Golterman, Nucl. Phys. **B273**, 663 (1986).

[20] M. L. Golterman and J. Smit, Nucl. Phys. **B255**, 328 (1985).

[21] G. Kilcup, in *Lattice '89* [9], p. 533.

[22] M. Fukugita, H. Mino, M. Okawa, and A. Ukawa, Phys. Rev. Lett. **68**, 761 (1992); M. Fukugita, N. Ishizuka, H. Mino, M. Okawa, and A. Ukawa, in *Lattice '91* [3], p. 265.

[23] S. Gottlieb, W. Liu, D. Toussaint, R. L. Renken, and R. L. Sugar, Phys. Rev. D **36**, 3797 (1987).

[24] We also note that our runs on a 16^4 lattice produced results consistent with those of Ref. [4] which used a smaller step size and a more stringent stopping condition.

[25] G. W. Kilcup and S. R. Sharpe, Nucl. Phys. **B283**, 493 (1987).

[26] K. C. Bowler, C. B. Chalmers, R. D. Kenway, D. Roweth, and D. Stephenson, Nucl. Phys. **B296**, 732 (1988).

[27] N. Ishizuka, M. Fukugita, H. Mino, M. Okawa, and A. Ukawa, in *Lattice '91* [3], p. 284; Report No. KEK-TH-351, 1993 (unpublished).

[28] V. N. Gribov, Nucl. Phys. **B139**, 1 (1978).
[29] Ph. de Forcrand, J. E. Hetrick, A. Nakamura, and M. Plewnia, in *Lattice '90* [4], p. 194; E. Marinari, R. Ricci, and C. Parrinello, *ibid.*, p. 199.
[30] B. Efron, SIAM Rev. **21**, 460 (1979); R. G. Miller, Biometrika **61**, 1 (1974).
[31] A. Krasnitz, Phys. Rev. D **42**, 1301 (1990); in *Lattice '90* [4], p. 40.
[32] For the lattices with spatial sizes $L=8$ and 12 at $\beta=5.7$ our fits with the covariance matrix led to the undesirable result that the fitting curves fall below the propagator data (the fitted hadron mass values deviate by one to one and a half standard deviations from those using only the diagonal elements of the covariance matrix). The statistical quality of the covariance matrix for $L=8$ and $L=12$ is poor compared to that for $L=20$. In fact the errors of small eigenvalues of the matrix estimated by the jack-knife method is 90% ($L=8$), 50% ($L=12$), and 15% ($L=20$). It is possible that large statistical fluctuations have accidentally boosted the off-diagonal elements of the covariance matrix relative to the diagonal ones, which would render the significance of the fits doubtful. We therefore decided not to adopt fits with the full covariance matrix for small lattices. For the $L=20$ lattice on the other hand we do not observe a systematic deviation between the fitting curves and the data; in fact the fits using only the diagonal elements of the covariance matrix give results consistent with those obtained with the full covariance matrix.
[33] We have made a systematic study of the operator dependence of the baryon masses with the quenched approximation [27]. The wall source is constructed so that it matches the hadron operator. In this study the masses for $B(\mathrm{VII}_2)$ and $B(\mathrm{X}_1)$ are consistent with those for $B(\mathrm{VII}_1)$ and $B(\mathrm{X}_2)$, and show the value of the nucleon mass. On the other hand, the mass for $B(\mathrm{V})$ exhibits a higher value, consistent with the Δ mass. In our present study we could not obtain a good signal-to-noise ratio for $B(\mathrm{V})$.
[34] A similar pattern of variation is also found with quenched simulations, where much higher statistics is more easily attainable [27].
[35] H. Sharatchandra, H. J. Thun, and P. Weisz, Nucl. Phys. **B192**, 205 (1981).
[36] M. F. L. Golterman and J. Smit, Nucl. Phys. **B245**, 61 (1984).
[37] J. Gässer and H. Leutwyler, Phys. Rep. **87**, 77 (1982).
[38] A. Gonzalez-Arroyo, F. J. Yndurain, and G. Martinelli, Phys. Lett. **117B**, 437 (1982); H. W. Hamber and C. M. Wu, Phys. Lett. **133B**, 351 (1983).
[39] G. Höhler *et al.*, *Handbook of Pion-Nucleon Scattering* (Fach-Informations-Zentrum, Karlsruhe, 1979), p. 426.
[40] M. Fukugita, H. Mino, M. Okawa, G. Parisi, and A. Ukawa, Phys. Lett. B **294**, 380 (1992).
[41] This argument is not directly applicable for baryons because of the nonzero minimum momentum π/L for the antiperiodic boundary condition.
[42] MILC Collaboration, C. Bernard *et al.*, in *Lattice '91* [3], p. 262; S. Gottlieb, W. Liu, D. Toussaint, R. L. Renken, and R. L. Sugar, Phys. Rev. Lett. **59**, 1513 (1987).
[43] C. DeTar and J. B. Kogut, Phys. Rev. D **36**, 2828 (1987).
[44] S. Ono, Phys. Rev. D **17**, 888 (1978).
[45] See, for example, A. Ukawa, in *Proceedings of the XXVth International Conference on High Energy Physics,* Singapore, 1990, edited by K. K. Phua and Y. Yamaguchi (World Scientific, Singapore, 1991), p. 79.
[46] S. Gottlieb *et al.*, in *Lattice '91* [3], p. 308.
[47] M. Fukugita, N. Ishizuka, H. Mino, M. Okawa, and A. Ukawa, Phys. Lett. B **301**, 224 (1993).
[48] D. Daniel and S. N. Sheard, Nucl. Phys. **B302**, 471 (1988).
[49] N. Ishizuka and Y. Shizawa (in preparation).